ELSEVIER

Journal of South American Earth Sciences 18 (2005) 237–254

Journal of
South American
Earth Sciences

www.elsevier.com/locate/jsames

Potassic and low- and high-Ti mildly alkaline volcanism in the Neoproterozoic Ramada Plateau, southernmost Brazil

Carlos Augusto Sommer[a,*], Evandro Fernandes de Lima[b], Lauro Valentim Stoll Nardi[b], Ana Maria Graciano Figueiredo[c], Ronaldo Pierosan[a]

[a]*Instituto de Geociências, Universidade Federal do Rio Grande do Sul (UFRGS), Av. Bento Gonçalves 9500, Cx. Postal 15001, CEP 91501-970 Porto Alegre, RS, Brazil*

[b]*Centro de Estudos em Petrologia e Geoquímica/PRONEX/UFRGS, Av. Bento Gonçalves 9500, Cx. Postal 15001, CEP 91501-970 Porto Alegre, RS, Brazil*

[c]*IPEN/CNEN-SP, Av. Bento Gonçalves 9500, Cx. Postal 15001, CEP 91501-970 Porto Alegre, RS, Brazil*

Received 1 May 2003; accepted 1 November 2004

Abstract

Ramada Plateau Neoproterozoic volcanism represents a portion of the shoshonitic and mildly alkaline magmatism related to postcollisional events of the Brasiliano/Pan African cycle of southernmost Brazil. It is constituted by shoshonitic basic-intermediate lavas, followed by a bimodal sequence characterized by pyroclastic deposits, lava flows, and hypabyssal rocks with ages of 549 ± 5 Ma. The shoshonitic magmatism presents greater K_2O than Na_2O_2, K_2O/Na_2O ratios close to 1, and moderate large ion lithophile and high-field strength element contents. The bimodal basic-acid volcanism presents a transitional chemical affinity with features of sodic, silica-saturated alkaline to continental tholeiitic series. Observed basic and acid rocks with contrasting Ti contents are referred to as high- and low-Ti basalt-rhyolites. Another group of acid rocks with higher Nb, Ta, and Rb values was identified as high-Nb rhyolites. The Ramada Plateau magmatism is comparable to associations related to the final stages of orogenic cycles, in which shoshonitic and high- and low-Ti alkaline magmatism reflects the melting of subduction-modified sources, whereas the high-Nb magmas show less influence of subduction-related metasomatism and are closer to magmas produced from anorogenic sources. A model of magma generation in collisional settings involving slab break-off and asthenospheric upwelling is applied to the evolution of magmatism from subduction-related to anorogenic in the Ramada Plateau.

Keywords: Bimodal volcanism; Mildly alkaline magmatism; Postcollisional settings; Shoshonites

1. Introduction

Shield areas in southern Brazil are composed mostly of magmatic rocks related to the Brasiliano/Pan African cycle emplaced in a metamorphic basement of Paleoproterozoic age (Hartmann et al., 1999; Soliani et al., 2000). The Brasiliano/Pan-African cycle is marked by arc magmatism aged mainly 700–760 Ma (Fernandes et al., 1992; Babinski et al., 1997; Chemale, 2000) and widespread postcollisional magmatism, in the sense of Liégeois (1998), aged 650–550 Ma (Bitencourt and Nardi, 2000). The postcollisional stage in the eastern portion of the region is marked by the southern Brazilian shear belt with voluminous magmatism, which constitutes the Pelotas batholith (Phillip et al., 2000) that includes syntranscurrent, high-K, calc-alkaline granitoids and leucocratic peraluminous granites that evolve to granitoids with shoshonitic affinity and eventually to late- to posttranscurrent, dominantly metaluminous alkaline granites. Other than the leucocratic peraluminous granites, all granitoid types are associated with the basic magmatism represented by mafic microgranular enclaves, dykes, and mafic components in comingling systems. Continental tholeiitic and mildly alkaline basaltic magmas were identified among these mafic components (Bitencourt and Nardi, 2000).

* Corresponding author. Fax: +55 51 3316 7302.
E-mail address: casommer@sinos.net (C.A. Sommer).

0895-9811/$ - see front matter © 2005 Elsevier Ltd. All rights reserved.
doi:10.1016/j.jsames.2004.11.003

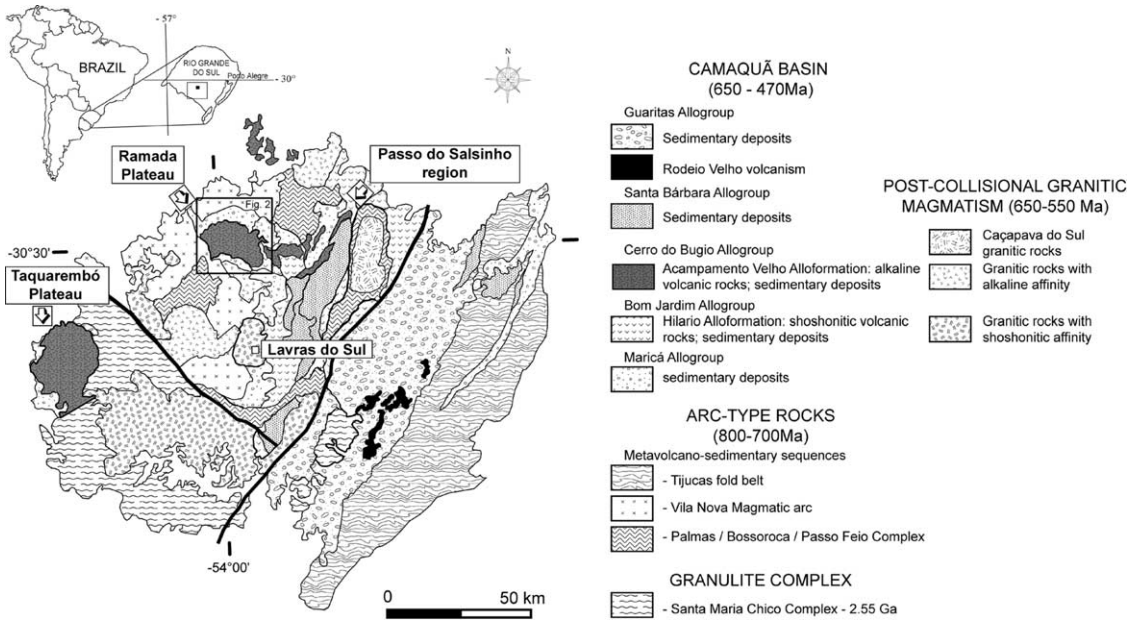

Fig. 1. Simplified geological map of the Sul Rio Grandense shield and main occurrence of Acampamento Velho volcanism (modified from Paim et al., 2000; Wildner et al., 2002).

The western and northwestern portions of the region represent less deformed areas, with volcanosedimentary sequences in the Camaquã basin (Fig. 1) deposited during this time interval (650–550 Ma) and intruded by plutonic associations with the same geochemical evolution as is observed in the eastern part. High-K, calc-alkaline granitoids, shoshonitic plutonovolcanic associations, and silica-saturated alkaline to continental tholeiitic plutonovolcanic sequences show ages varying from approximately 650 to 570 Ma. The sedimentary sequences, which are included with the coeval magmatism in the Camaquã basin, evolve from shallow marine in the Maricá Allogroup to lacustrine and alluvial in the Bom Jardim and Cerro do Bugio Allogroups (Paim et al., 2000). Magmatism in the Bom Jardim Allogroup is related to the Lavras do Sul shoshonitic association, which is composed of plutonic and volcanic basic to acid rocks with ages of 610–590 Ma (Lima and Nardi, 1998). Voluminous sodic, silica-saturated, alkaline magmatism composed mostly of metaluminous granites with minor peralkaline granites and dioritic rocks is related to the Saibro intrusive suite (Nardi and Bonin, 1991). Cogenetic with these intrusives, the volcanic rocks of the Acampamento Velho Alloformation (Cerro do Bugio Allogroup) (Fig. 1) occur in large volcanic plateaus composed mostly of acid lavas and pyroclastics with minor intermediate and basic components (Sommer et al., 1999; Wildner et al., 1999; Almeida et al., 2002).

The last postcollisional events related to the Brasiliano/Pan African cycle (Brito Neves and Cordani, 1991) are represented by transcurrent tectonics along relatively narrow shear belts with associated magmatism, such as the Caçapava granitic complex (Nardi and Bitencourt, 1989) at approximately 550 Ma, and less voluminous alkaline magmatism with similar ages.

In this article, we present the results of an integrated petrographic, geochemical, and geochronological study performed on the Neoproterozoic Ramada Plateau volcanic rocks in southernmost Brazil to contribute to the petrological characterization of volcanic associations that occur in postcollisional tectonic settings.

2. Geology of the Ramada Plateau

The Ramada Plateau, situated in the western portion of the Sul Rio Grandense shield, is characterized by a nondeformed basic-acid volcanic succession and related subvolcanic intrusions in the Neoproterozoic III, Hilario, and Acampamento Velho Alloformations (Paim et al., 2000) of the Camaquã basin. The country rocks of the volcanic plateau include metamorphosed tonalitic associations and basic–ultrabasic intrusive associations, interpreted as related to a continental crust with a juvenile isotopic signature (Chemale, 2000), and Neoproterozoic sedimentary rocks included in the Maricá Allogroup. The Plateau is intruded by alkaline granitoids of the Ramada intrusive complex (Gastal and Lafon, 1998) and partially covered by Gondwana sedimentary rocks (Fig. 2).

The Ramada Plateau covers an area of 24 km (E–W) by 12 km (N–S) and is approximately 120 m high, constituted mainly of acidic pyroclastic flow deposits, acid-basic lava flows, and shallow intrusions. Its lower portion is represented by andesitic lava flow deposits, succeeded by

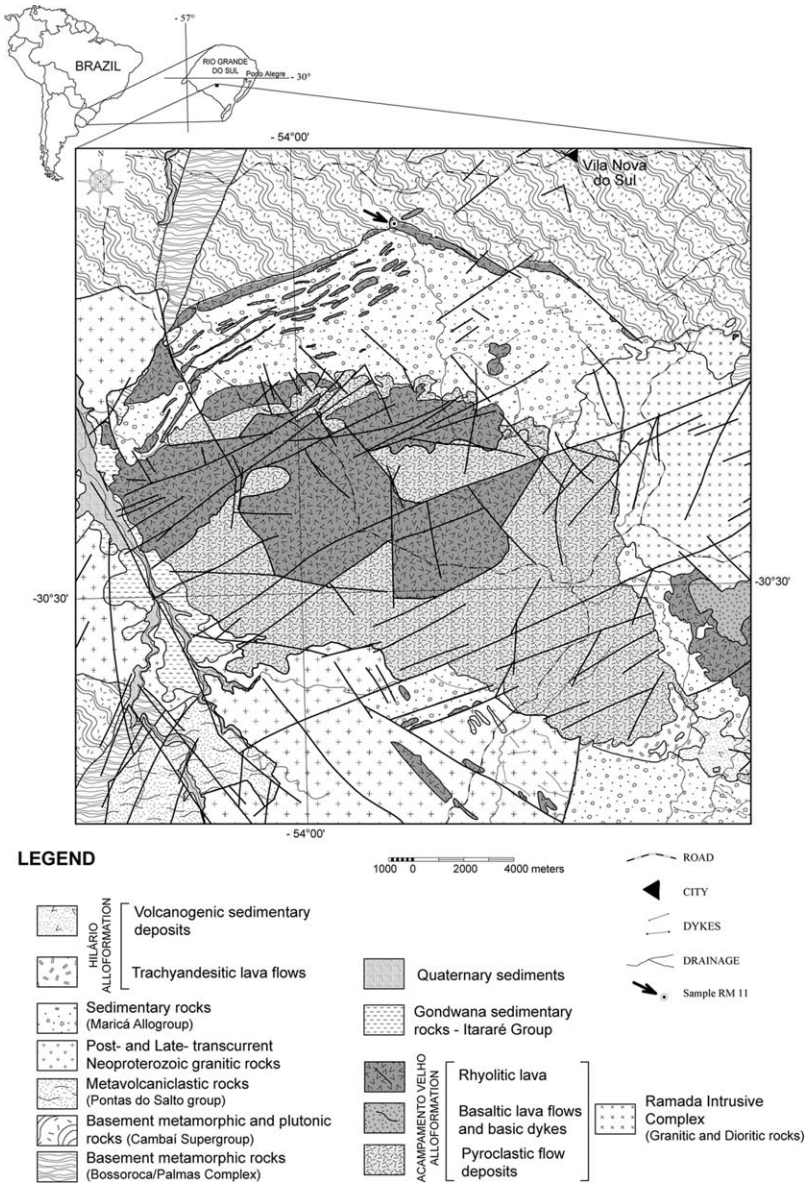

Fig. 2. Localization and geological map of the Ramada Plateau region.

volcanogenic conglomerates (Fig. 3) observed mainly in the eastern part of the plateau (Hilario Alloformation). This unit is succeeded by bimodal volcanism (Acampamento Velho Alloformation) characterized by (Fig. 3): (1) acid pyroclastic flow deposits in near-horizontal layers (60–80 m thick), characterized as co-ignimbrite breccias and lenticulite-type and crystal-rich ignimbrites; (2) basic dykes (1–3 m thick) that cut the pyroclastic sequence; (3) rhyolitic lava flows (20–30 m thick) that overlie the pyroclastic deposits with complex flow foliation, probably erupted along fractured zones; and (4) basaltic lava flows intercalated with the upper acidic lava flow sequence and restricted to a small portion in the northwest of the plateau.

Subvolcanic acid intrusions cut the andesitic basal unit and country rocks around the Ramada Plateau. Dykes and sills (1–5 m thick) are the dominant intrusions, though NW–SE- and NE–SW-oriented larger bodies are observed. Fluorite and galena vein mineralization is associated with some subvolcanic intrusions (Rocha et al., 1999). Some of these rocks have been studied by Matos et al. (2002) in the Santuário region (north of the plateau) and related to the volcanic rocks of the Ramada Plateau. These subvolcanic intrusions lie below a complex system of ancient vents for volcanism of the Ramada Plateau.

3. Petrography of the volcanic deposits

Flows in the basal unit are represented by basaltic trachyandesites with an incipient flow orientation, porphyritic and glomeroporphyritic textures with abundant andesine-labradorite ($An_{37–52}$) phenocrysts, minor amounts

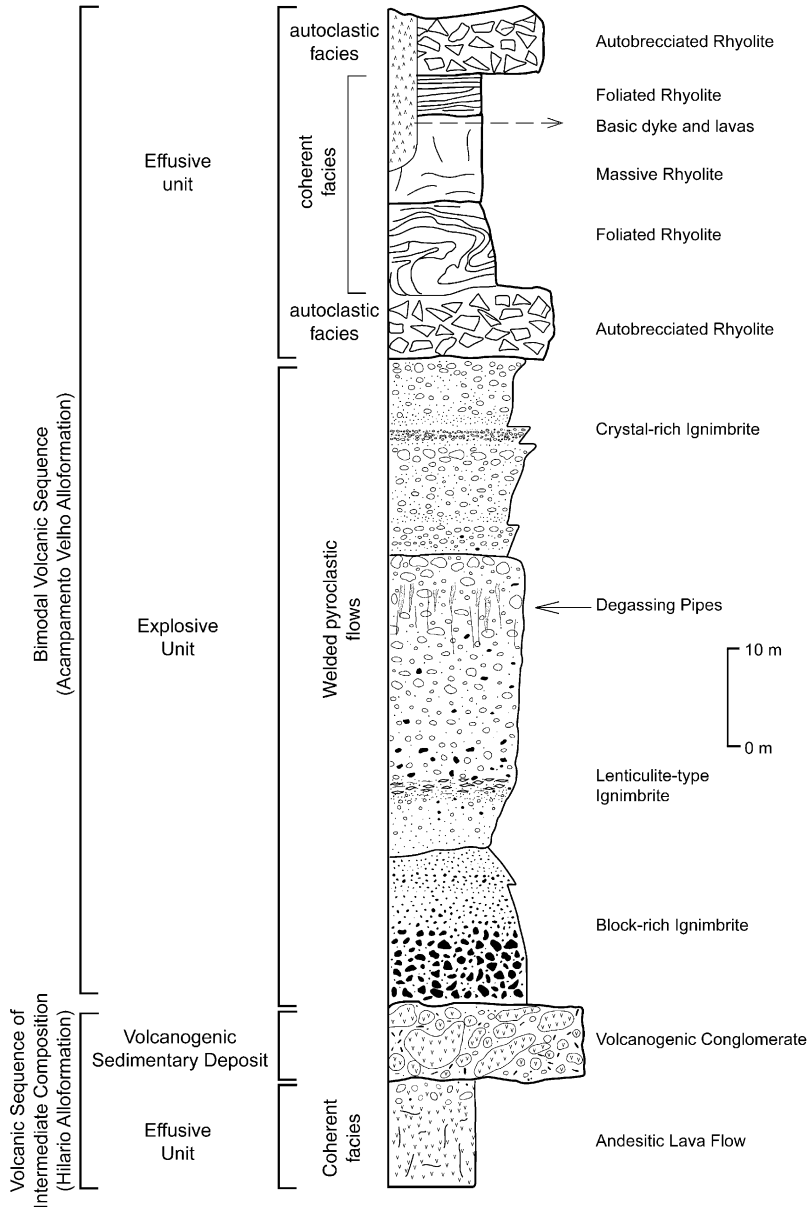

Fig. 3. Schematic representation of the Ramada Plateau stratigraphic section.

of augite ($Wo_{39–41}$, $En_{45–46}$, $Fs_{13–17}$), Ti-magnetite, apatite, and remnants of olivine. Andesine-labradorite crystallites, microlites, and glass constitute the groundmass. Some plagioclase grains exhibit tabular forms and sieve textures that indicate fast cooling. Carbonates, chlorite, iddingsite, boulingite, iron oxides, and white mica are common secondary minerals.

Pyroclastic flow deposits are represented by ignimbrites and co-ignimbrite breccias of comenditic nature. The former constitutes the most abundant deposit in the Ramada Plateau. The proximal and basal facies are characterized by co-ignimbritic breccias, with dominant juvenile and accidental blocks and lapilli in a tuffaceous matrix. This facies shows lateral gradational changes to ignimbrites with abundant lithoclasts and pumice lapillis, in addition to K-feldspar and quartz phenoclasts. Ignimbrites are separated into two main lithofacies: lenticulites and crystal-rich deposits. The lenticulites have K-feldspar and quartz phenoclasts, pumice fragments, and scarce lapilli-size lithoclasts in an abundant vitroclastic matrix. The lenticular aspect and eutaxitic texture are due to the high-grade welding of the deposit. Axiolites and spherulites, common features of high-temperature devitrification processes, are observed mainly in pumice fragments. In some of the upper portions of the unit, typical features of degassing pipes (fumaroles) occur, characterized by centimeter-sized circular structures filled by clay, which grade upward to brecciated zones. These structures originated during the deposit cooling from the escape of gas (Sheridan, 1970; Cas and Wright, 1987; McPhie et al., 1993).

Thin layers (0.4–0.6 m) of crystal-rich ignimbrite overlie the lenticulites (Sommer et al., 2001) and have high crystal content (50–60%). K-feldspar (0.5–2.5 mm) and quartz (1–2 mm) phenoclasts, scarce pumice, and accidental and cognate lithoclasts occur in an ash-sized matrix of mainly shards. Weak welding of the deposit generates incipient eutaxitic texture. The high crystal concentration in pyroclastic flow deposits can be related to eruptions of highly crystallized magmas or physical fractionation during flow (Cas and Wright, 1987).

The Ramada Plateau pyroclastic flow deposits show evidence of hot, gas-supported emplacement, such as welding, high-temperature devitrification processes (spherulites, axiolites), lithophysae, perlitic fractures, gas-escape structures, and vapor-phase crystals. This evidence suggests deposition through primary pyroclastic flows, which usually are restricted to subaerial and shallow-water settings (McPhie et al., 1993).

Basic rocks in the Ramada Plateau occur as dykes and lava flow deposits of hawaiitic and mugearitic basalt. The mineralogical composition is similar in both lithologies, but small textural differences are observed. Dykes show a fine phaneritic texture with plagioclase, clinopyroxene, ilmenite, and olivine remnants. Some plagioclase grains have sieve texture and zoning. Lavas are porphyrytic to glomeroporphyritic with abundant plagioclase and pyroxene phenocrysts in a matrix of plagioclase-pyroxene crystallites and microlites, as well as cryptocrystalline-transformed glass. Labradorite ($An_{44–67}$) is the common composition of plagioclase, but albite ($An_{1–9}$) is found in some dyke samples, probably due to albitization of an originally more calcic plagioclase. Clinopyroxenes are augite ($Wo_{39–43}$, $En_{38–48}$, $Fs_{12–20}$) in the dykes and diopside ($Wo_{48–49}$, $En_{28–37}$, $Fs_{14–23}$) in the lava flows (Morimoto, 1988). In the dykes, the clinopyroxenes have higher concentrations of TiO_2, Al_2O_3, and Na_2O than in the lavas. Carbonate, chlorite, serpentine, iron oxides, and white mica are the main secondary phases.

Acid lava flows and synvolcanic intrusions are represented mainly by comenditic rhyolites and minor trachytes. They occur along lineaments (fissure zones, probably old linear vents), where they exhibit a near-vertical flow foliation, laterally gradating to autobreccias, lavas with near-horizontal flow foliation, and massive textures. Three main textural groups were identified: hemicrystalline, microcrystalline, and spherulite. Their relationships are complex and can be related to the heterogeneity of the crystallization and devitrification processes in these rocks (Matos et al., 2002). Acid lavas and intrusive rocks are composed of alkali feldspar, usually microperthite, quartz, and zircon, with iron oxides as accessory phases. Plagioclase, amphibole, and remnants of pyroxene are common in the intrusions and scarce in the plateau lavas. The relative proportions of minerals and their degree of preservation vary among the textural groups.

The hemicrystalline group has low percentages of microphenocrysts (ca. 5%) in a mosaic of quartz and feldspar microlites, crystallites, and cryptocrystalline-transformed glass, and perlitic Y-like fractures are observed. Quartz phenocrysts frequently show resorption features, such as embayed and roughly rounded shapes. Alkali feldspar is normally tabular. Mafic phases are mainly acicular crystals of amphibole and scarce pyroxene relicts partially replaced by amphibole and chlorite.

The microcrystalline group shows porphyritic and glomerporphyritic textures with quartz and feldspar phenocrysts in a hypidiomorphic quartz–feldspathic matrix. Granophyric texture is frequently observed around feldspar phenocrysts. Mafic phases are similar to those described in the previous group, and fluorite microcrysts are dispersed in the matrix of some intrusive rocks.

The spherulitic group is normally associated with the hemicrystalline rocks and has spherical radiating arrays of quartz–feldspar fibers, generally around quartz nuclei set in a quartz–feldspar micrographic matrix. Spherulites are a characteristic product of the high-temperature devitrification of natural glass, and their morphology varies according to the temperature or degree of undercooling that prevailed during their formation (Lofgren, 1971, 1974).

Amphiboles of acid rocks are calcic to sodic-calcic (Leake et al., 1997). The sodic-calcic phases are ferrowinchite, ferrobarroisite, and ferrorichterite, whereas the calcic one is ferroactinolite. According to Strong and Taylor (1984), Al-poor and Fe-rich sodic-calcic amphiboles are primary igneous amphiboles found in comenditic more often than in pantelleritic rocks, where arfvedsonite and riebeckite are typical phases (Nicholls and Carmichael, 1969). Experimental studies of amphibole crystallization suggest that the compositional evolution from calcic to sodic-calcic and sodic phases is due to a decrease in temperature and oxygen fugacity (Mitchell, 1990).

In the acid rocks, the composition of the potassic phase of microperthite is orthoclase ($Or_{84–98}$) and scarce homogeneous alkali feldspar grains with $Or_{41–47}$ compositions. Plagioclase is $An_{0.5–3}$ and probably represents late-magmatic reequilibrated compositions.

Opaque minerals are microphenocrysts of Ti-magnetite ($Usp_{0.54–0.62}$) and ilmenite ($Hem_{0.01–0.12}$) with compositions similar to those of peralkaline rhyolites from Pantelleria, Italy (Sutherland, 1975). The composition of magnetite–ilmenite pairs from hypabyssal rhyolites of this sequence suggests that they crystallized at temperatures of 850–886 °C, at oxygen fugacity of 10^{-14} bar, and between the NNO and QFM buffers (Matos et al., 2002).

4. Geochronology

We performed new sensitive high-resolution ion microprobe (SHRIMP) U–Pb dating of zircon grains from the hypabyssal rhyolitic rocks of the Ramada Plateau (sample RM-11; Fig. 2, Table 1). Zircon analyses were performed at the Research School of Earth Sciences Laboratory,

Table 1
SHRIMP U–Pb zircon data from Ramada Plateau hypabyssal rhyolites (sample RM11)

Grain spot	% $^{206}Pb_c$	ppm U	ppm Th	$^{232}Th/^{238}U$	ppm $^{206}Pb^*$	(1) $^{206}Pb/^{238}U$ age	(1) $^{207}Pb/^{206}Pb$ age	% Dis-cordant	(1) $^{207}Pb^*/^{206}Pb^*$	± %	(1) $^{207}Pb^*/^{235}U$	± %	(1) $^{206}Pb^*/^{238}U$	± %	Err. corr.
1.1	0.00	165	115	0.72	12.9	562.7 ± 9.4	578 ± 38	3	0.0593	1.7	0.746	2.5	0.0912	1.8	0.710
2.1	0.16	202	114	0.58	15.5	550.5 ± 5.6	577 ± 40	5	0.0593	1.8	0.728	2.1	0.08914	1.1	0.500
3.1	0.39	131	88	0.69	10.4	565.6 ± 6.8	499 ± 78	−12	0.0572	3.5	0.723	3.8	0.0917	1.2	0.332
6.1	0.51	457	367	0.83	35.7	557.7 ± 4.7	566 ± 50	1	0.0590	2.3	0.735	2.5	0.09037	0.87	0.353
8.1	0.00	120	87	0.75	9.08	544.4 ± 6.6	559 ± 45	3	0.0588	2.1	0.714	2.4	0.0881	1.3	0.526
11.1	0.00	57	34	0.62	4.64	588.9 ± 9.5	640 ± 63	9	0.0610	2.9	0.805	3.4	0.0957	1.7	0.503
11.2	0.00	138	98	0.74	10.3	536.2 ± 6.4	564 ± 44	5	0.0589	2.0	0.705	2.4	0.0867	1.2	0.527
13.1	0.61	82	53	0.67	6.22	543.6 ± 8.0	443 ± 110	−19	0.0558	5.0	0.676	5.2	0.0880	1.5	0.293
15.1	0.74	50	25	0.51	3.94	567 ± 12	704 ± 130	24	0.0629	6.3	0.797	6.7	0.0920	2.3	0.340
16.1	0.11	114	40	0.37	33.2	1,876 ± 20	1,971 ± 16	5	0.1210	0.92	5.635	1.5	0.3379	1.2	0.800
17.1	0.00	69	44	0.66	5.13	534.1 ± 8.7	547 ± 76	2	0.0585	3.5	0.696	3.9	0.0864	1.7	0.440
17.2	0.33	326	234	0.74	25.0	549.5 ± 4.9	548 ± 44	0	0.0585	2.0	0.718	2.2	0.08897	0.93	0.421
18.1	0.00	84	47	0.58	6.50	557 ± 10	666 ± 52	20	0.0618	2.4	0.768	3.1	0.0902	1.9	0.623
20.1	0.05	618	506	0.85	46.7	543.1 ± 4.3	559 ± 21	3	0.05879	0.98	0.7125	1.3	0.08791	0.82	0.643

Errors are 1σ; Pb_c and Pb^* indicate the common and radiogenic lead, respectively. Error in standard calibration was 0.33% (required when comparing data from different mounts). (1) Common Pb corrected using measured ^{204}Pb. Note that analysis 17.2 is sited on grain no. 18.

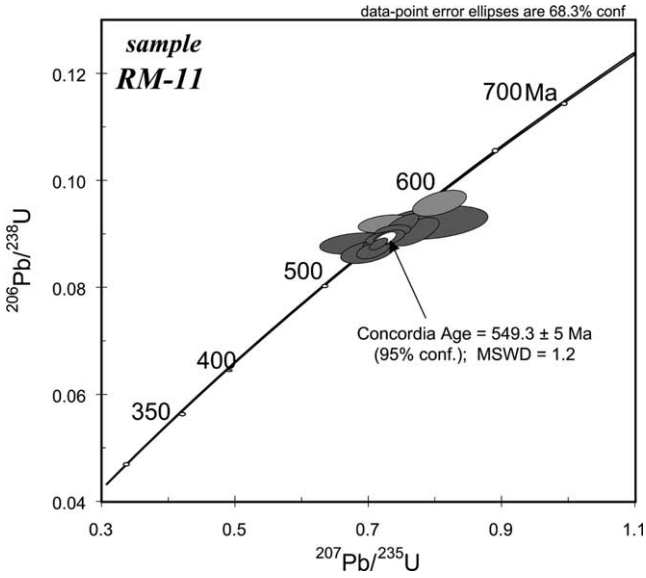

Fig. 4. U–Pb diagram displaying concordia obtained from zircon of Ramada Plateau rhyolitic rocks.

Australian National University, by Richard Amstrong. The zircons were mounted and polished in standard epoxy cement and then carbon-coated for backscattered electron and cathodoluminescence analysis to define the internal structure of the crystals. The mount was later repolished and coated with gold for the SHRIMP microanalytical isotopic determinations. The isotopic U–Pb analyses were obtained with SHRIMP II; instrumental conditions and data acquisitions were as described by Compston et al. (1984, 1992). Fifteen zircon spots were analyzed, and one standard determination was obtained for each of three analyses.

After data reduction, eleven points plotted close to the concordia curve and yielded an average age (2σ criteria; MSWD = 1.2) of 549.3 ± 5 Ma (Fig. 4), with age uncertainties at the 95% confidence level for the concordant population. Previous data have indicated ages of 573 ± 18 Ma in zircon for the Acampamento Velho subalkaline rhyolite of the Passo do Salsinho region (Chemale, 2000; Almeida et al., 2002) and 572 ± 3 Ma in zircon from the cogenetic intrusive association of the Taquarembó Plateau region (Gastal and Lafon, 2001; Fig. 1).

5. Geochemical features of the volcanic and subvolcanic rocks

5.1. Analytical procedures

Geochemical studies in the volcanic and subvolcanic intrusive rocks of the Ramada Plateau were based on 49 whole-rock samples, analyzed for major and trace elements (Table 2). Twelve samples were analyzed by Activation Laboratories Ltd, Ontario, Canada, by inductively coupled plasma optical emission analysis for major

Table 2
Chemical analyses for major (wt%) and trace (ppm) elements for representative whole-rock samples

Sample	Rm32-c	Rm33-a	Rm15-a	Rm27-a	Rm57-f–c	Rm80-d–c	Rm31	R-m171-c	Rm11-a	Rm10-a	R-m183-c	Rm25-b	Rm20-c	Rm14-a	4050a	Rm23-a	Ma-p4011-c	Rm78-c	Rm45-a	Rm74	Rm09-a–c	4051a	Rm36
Lat.	30°26-′16″	30°26-′13″	30°30-′01″	30°30-′22″	30°28-′14″	30°29-′24″	30°26-′08″	30°26-′14″	30°22-′05″	30°22-′01″	30°23-′26″	30°31-′09″	30°33-′13″	30°29-′27″	30°25-′15″	30°31-′04″	30°23-′33″	30°28-′13″	30°26-′00″	30°27-′29″	30°25-′17″	30°25-′08″	30°26-′25″
Long.	53°54-′06″	53°54-′13″	53°49-′29″	53°49-′16″	54°03-′08″	54°00-′05″	53°54-′05″	53°53-′16″	53°57-′01′	53°56-′33″	53°59-′01″	53°48-′07″	53°42-′24″	53°50-′12″	53°57-′26″	53°45-′20″	53°59-′00″	53°58-′35″	54°00-′14″	54°00-′33″	54°01-′17″	53°58-′35″	53°54-′16″
	1 *	1 *	2 *	2 *	3 **	3 **	4 (a) *	4 (a) **	4 (a) *	4 (a) *	4 (a) **	4 (b) *	4 (b) **	4 (b) *	4 (c) **	4 (c) *	5 (a) **	5 (b) **	6 (a) *	6 (a) **	6 (a) **	5 (b) **	6 (b) *
SiO_2	52.87	53.74	47.29	47.73	46.26	51.70	63.83	69.66	73.94	74.68	73.82	72.03	75.68	73.12	77.02	72.54	75.05	74.91	72.13	75.85	77.26	79.63	71.50
TiO_2	1.24	1.11	1.73	1.81	2.69	1.55	0.73	0.37	0.20	0.20	0.23	0.25	0.23	0.27	0.17	0.23	0.12	0.12	0.11	0.04	0.03	0.09	0.11
Al_2O_3	14.50	15.42	17.17	17.84	15.59	14.84	14.56	14.73	11.88	12.03	12.58	11.69	12.45	11.83	11.39	11.86	13.19	12.08	12.90	12.68	11.40	10.64	13.39
Fe_2O_3	10.50	8.00	13.86	11.18	11.42	10.94	4.60	2.81	2.69	2.16	3.06	3.23	2.42	3.38	2.32	3.15	1.99	1.93	2.41	1.32	1.01	1.86	1.56
MnO	0.17	0.16	0.24	0.28	0.19	0.17	0.07	0.04	0.08	0.02	0.02	0.09	0.05	0.08	0.02	0.05	0.01	0.03	0.01	0.01	0.01	0.02	0.02
MgO	5.43	5.78	4.02	4.52	4.36	5.69	1.79	0.62	0.15	0.15	0.25	0.21	0.25	0.25	0.06	0.24	0.10	0.09	0.12	0.05	0.04	0.03	0.14
CaO	5.45	6.91	8.68	8.50	9.10	5.56	2.75	1.28	0.07	0.06	0.01	0.90	0.06	0.46	0.06	0.76	0.07	0.41	0.02	0.02	0.01	0.01	0.58
Na_2O	3.28	2.76	3.86	4.13	3.28	3.95	4.05	3.37	3.64	3.43	3.65	3.87	5.80	3.88	3.70	3.72	3.69	4.21	3.05	4.09	0.25	3.29	4.66
K_2O	3.36	3.22	0.76	0.98	0.91	1.64	4.24	4.48	4.98	5.11	3.93	5.21	0.54	5.32	3.76	5.11	4.21	4.51	5.36	4.22	9.21	3.91	4.68
P_2O_5	0.44	0.40	0.23	0.23	0.79	0.98	0.16	0.09	0.03	0.02	0.04	0.03	0.05	0.03	0.05	0.04	0.03	0.02	0.01	0.04	0.02	0.03	0.03
LOI	2.50	1.80	1.20	2.60	5.23	3.39	2.30	1.56	1.40	1.00	1.61	1.80	1.78	0.80	1.22	1.90	1.37	0.67	1.70	0.99	0.83	0.67	1.10
Total	99.74	99.30	99.04	99.80	99.82	100.41	99.08	99.01	99.06	98.86	99.20	99.31	99.32	99.42	99.77	99.60	99.83	98.99	97.82	99.31	100.07	100.18	97.77
Ba	120	1011	241	178	542	933	1069	1070	171	158	302	137	172	127	98	272	412	55	54	71	67	56	179
Rb	86	75	22	33	14	35	79	91	92	93	101	123	7	82	108	99	128	144	261	315	446	118	250
Sr	495	671	437	496	482	458	233	173	10	10	20	135	105	15	32	25	27	9	7	6	6	10	20
Ga	22	22	18	18	18	21	20	16	27	29	25	22	27	24	22	26	28	28	36	35	15	20	37
Nb	14	15	6	7	14	18	21	13	38	42	55	25	30	35	23	41	35	37	81	67	58	19	79
Zr	252	200	140	130	174	259	372	305	674	672	739	352	621	914	447	682	306	491	299	278	437	233	385
Y	24	23	24	22	41	50	36	28	57	63	94	42	69	55	80	69	92	126	84	101	125	77	101
La	51.0	52.0	12.5	12.3	35.5	58.0	74.0	48.1	117.0	107.0	92.9	145.0	169.0	173.0	59.1		68.8	48.9	5.6	1.4	0.8	30.4	25.5
Ce	100.0	103.0	29.3	29.1	74.6	112.0	135.0	84.2	238.0	221.0	181.0	283.0	298.0	329.0	95.3		148.0	104	20.9	10.0	6.9	60.1	74.0
Pr	–	–	–	–	9.7	13.8	–	8.9	–	–	21.0	–	37.6		14.6		18.5	13.3	–	0.7	0.4	7.98	–
Nd	48.0	49.0	16.0	16.0	39.0	51.9	52.0	31.5	101.0	89.0	79.9	117.0	132.0	131.0	55.2		74.9	49.9	9.9	2.9	1.9	30.8	39.0
Sm	8.6	8.4	5.0	4.6	9.0	10.9	8.7	5.4	19.0	19.0	16.5	19.0	23.4	21.0	13.5		19.6	15.9	4.4	2.3	1.9	9.4	16.0
Eu	2.0	2.1	1.9	1.6	2.4	2.7	1.6	0.9	0.6	0.7	0.6	0.9	0.9	1.0	0.2		0.1	0.3	0.1	0.1	0.1	0.09	0.2
Gd	–	–	–	–	8.7	10.1	–	4.3	–	–	15.3	–	17.8		13.2		19.0	17.8	–	4.7	5.0	10.4	–
Tb	0.9	0.7	0.9	0.6	1.5	1.7	1.0	0.8	2.7	2.7	3.0	2.4	2.6	2.4	2.6		3.5	3.7	2.1	1.8	2.5	2.4	3.8
Dy	–	–	–	–	7.5	8.7	–	4.7	–	–	16.9	–	13.5		15.3		17.7	22	–	13.6	21.6	14.3	–
Ho	–	–	–	–	1.5	1.7	–	1.0	–	–	3.5	–	2.7		3.1		3.3	4.6	–	3.4	5.2	2.9	–
Er	–	–	–	–	3.9	4.6	–	2.9	–	–	9.9	–	7.4		8.8		9.2	13.1	–	11.4	16.0	8.2	–
Tm	–	–	–	–	0.5	0.7	–	0.5	–	–	1.6	–	1.1		1.4		1.4	2	–	2.0	2.6	1.32	–
Yb	1.4	1.5	2.9	2.5	3.2	4.0	3.8	3.0	6.5	6.8	9.4	7.0	7.3	5.9	7.9		8.1	11.8	9.7	12.2	15.3	7.4	11.7
Lu	0.3	0.2	0.4	0.3	0.5	0.6	0.5	0.5	1.0	1.1	1.4	1.1	1.1	1.1	1.2		1.2	1.7	1.4	1.7	2.2	1.05	1.7
U	4.2	2.9	0.4	0.4	0.5	1.0	2.7	2.6	2.0	2.7	6.7	2.0	2.1	1.6	2.1		2.4	3.4	2.2	1.8	3.6	2.01	3.9
Th	12.4	11.6	0.7	1.0	2.0	4.6	10.2	10.4	12.0	11.8	20.4	12.7	12.2	12.1	16.7		14.7	14.5	17.4	18.2	17.3	11.3	18.4
Hf	5.9	5.7	3.6	3.7	4.4	6.4	8.6	0.5	13.6	14.0	18.2	16.3	15.4	16.3	14.2		10.4	17.2	11.2	14.7	11.7	8.1	14.9
Ta	0.8	0.9		0.1	1.1	1.1	1.6	1.1	1.9	1.8	29.2	1.8	1.6	1.6	1.8		2.5	2.5	5.8	5.3	4.1	1.5	4.9

(1) Shoshonitic intermediate rocks; (2) Low-Ti basic rocks; (3) High-Ti basic rocks; (4) High-Ti acid rocks: (a) hypabyssal, (b) lavas, and (c) ignimbrites; (5) Low-Ti acid rocks: (a) hypabyssal and (b) lavas; (6) High-Nb acid rocks: (a) lavas and (b) ignimbrites. *Analytical determinations performed by Geochemistry Laboratory, CPGq-UFRGS, Brazil, and Nuclear and Energetic Search Institute-IPEN, Brazil. **Analytical determinations performed by Activation Laboratories Ltd, Ontario, Canada. Analytical procedure described in the text. (–) Not determined.

elements and inductively coupled plasma mass spectrometry for trace elements. Thirty-seven samples were analyzed for major and trace elements (Rb, Ba, Sr, Ga, Nb, Y, and Zr) by the Geochemistry Laboratory, CPGq-UFRGS, Brazil, with X-ray fluorescence and atomic absorption spectrometry methods. From these, 12 samples were analyzed for rare-earth elements (REE; La, Ce, Nd, Sm, Eu, Tb, Yb, and Lu) and other trace elements (U, Th, Hf, Ta, Sc, Cs, Co, Ba, and Rb) by neutron activation, performed by Instituto de Pesquisas Energéticas e Nucleares-IPEN, São Paulo, Brazil.

The geochemical characterization of the Ramada magmatism was based mainly on low mobility elements because loss on ignition (LOI) values are high in some basic rocks, though correlation studies have indicated that there are no significant modifications of major elements in these samples. High LOI values were observed in samples with abundant secondary phases, such as carbonate, clay minerals, and chlorite.

In the acid association, our data interpretation was based mainly on lava flow samples. Ignimbrites with low contributions of cognates and accidental pyroclasts were used as additional data because their compositions are similar to that of acid lava.

5.2. Major- and trace-element geochemistry

Ramada Plateau volcanism is characterized by intermediate rocks of shoshonitic affinity, as well as a bimodal basic-acid association related to silica-saturated sodic alkaline series.

The shoshonitic intermediate lavas plot in the basaltic trachyandesite and shoshonite fields on a total alkali–silica (TAS) diagram (Le Bas et al., 1986), with $K_2O > (Na_2O_2)$ and a K_2O/Na_2O ratio close to 1 (Fig. 5). The shoshonitic

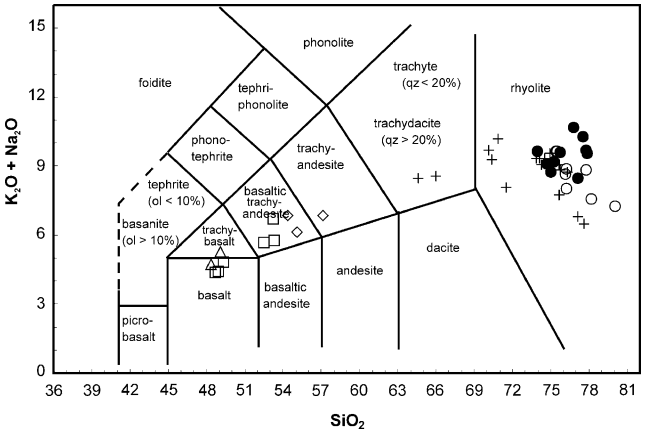

Fig. 5. Total alkali–silica diagram (Le Bas et al., 1986) of the volcanic and hypabyssal studied rock samples (data in wt%, volatile free). Diamonds: shoshonitic intermediate lavas; triangles: low-Ti basic lavas and dykes; squares: high-Ti basic lavas and dykes; circles: low-Ti acid lavas, hypabyssal rocks, and ignimbrites; crosses: high-Ti acid lavas, hypabyssal rocks, and ignimbrites; and filled circles: high-Nb acid lavas, hypabyssal rocks, and ignimbrites.

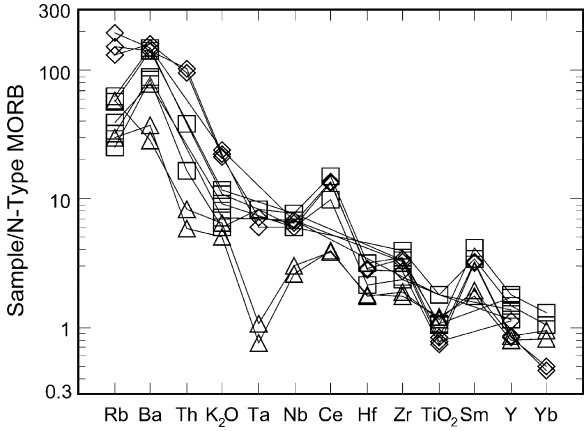

Fig. 6. N-MORB-normalized trace-element spidergrams for intermediate and basic rock samples. Diamonds: shoshonitic intermediate lavas; triangles: low-Ti basic lavas and dykes; squares: high-Ti basic lavas and dykes.

affinity of these rocks is corroborated by low TiO_2 (1.1–1.2wt%), CaO (5.2–6.9 wt%), and P_2O_5 (0.4–0.9 wt%) contents and relatively high Al_2O_3 (14.2–15.4 wt%), Rb (75–110 ppm), Ba (930–1050 ppm), and Sr (430–670 ppm) contents. The CIPW-norm calculations indicate that less differentiated shoshonitic rocks are metaluminous hypersthene trachybasalts and latites. The enrichment in large ion lithophile elements and LREE observed in mid-ocean ridge basalt (MORB)-normalized patterns are also characteristic of shoshonitic rocks (Morrison, 1980) (Fig. 6). Nb values are low in relation to LREE and K, which generally is considered typical of magmas generated from subduction-related sources (Kelemen et al., 1993). Chondrite-normalized REE patterns (Fig. 7) show Ce_N/Yb_N ratios close to 20 and an absence of Eu anomalies, typical of shoshonitic basic-intermediate rocks. These major and trace element data support shoshonitic associations (Morrison, 1980), similar to the volcanic rocks of the Lavras do Sul

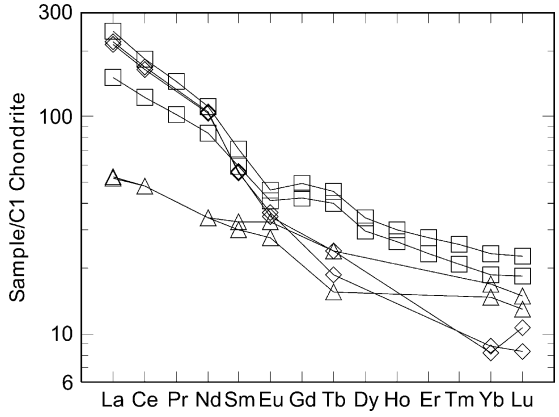

Fig. 7. Chondrite-normalized REE patterns for intermediate and basic rock samples. Diamonds: shoshonitic intermediate lavas; triangles: low-Ti basic lavas and dykes; squares: high-Ti basic lavas and dykes.

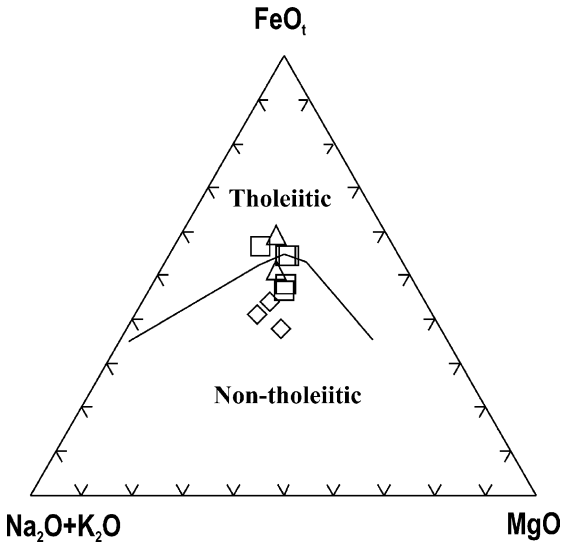

Fig. 8. Na_2O+K_2O–MgO–FeO_t diagram (modified from Irvine and Baragar, 1971) for intermediate and basic rock samples (data in wt%). Diamonds: shoshonitic intermediate lavas; triangles: low-Ti basic lavas and dykes; squares: high-Ti basic lavas and dykes.

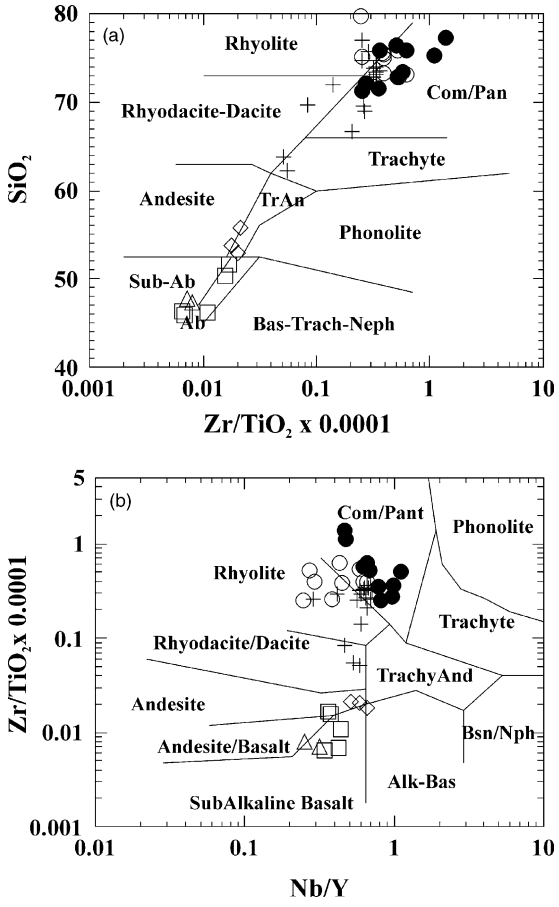

Fig. 9. Classification diagrams using incompatible elements for studied rock samples; fields after Winchester and Floyd (1977). Diamonds: shoshonitic intermediate lavas; triangles: low-Ti basic lavas and dykes; squares: high-Ti basic lavas and dykes; circles: low-Ti acid lavas, hypabyssal rocks, and ignimbrites; crosses: high-Ti acid lavas, hypabyssal rocks, and ignimbrites; and filled circles: high-Nb acid lavas, hypabyssal rocks, and ignimbrites. (a) $(Zr/TiO_2)\times0.0001$ versus SiO_2, and (b) Nb/Y versus $(Zr/TiO_2)\times0.0001$.

shoshonitic association (Lima and Nardi, 1998; Nardi and Lima, 2000).

The younger bimodal basic-acid association comprises volcanic and hypabyssal rocks whose compositional features are characteristic of silica-saturated sodic alkaline magmas or continental tholeiitic magmas. Trends in the AFM (Fig. 8) and TAS (Fig. 5) diagrams highlight this transitional composition. The sodic character is indicated by $(Na_2O_2)>K_2O$ values in samples that plot in the silica-saturated alkaline field, despite their high LOI values. Basic rocks are classified as hawaiites, mugearites, and subalkaline basalts, whereas acid rocks are dominantly comendites. The CIPW-norm calculations indicate that basic lavas are metaluminous olivine basalts, and some dykes are metaluminous quartz-normative trachytes with Na_2O/K_2O ratios close to 1.

The subalkaline to mildly alkaline affinity of the basic-acid association also is demonstrated by 'immobile' trace element diagrams, such as those based on the relationship of Zr/TiO_2 to SiO_2 or Nb/Y (Fig. 9), as suggested by Winchester and Floyd (1977). Their tholeiitic affinity is indicated by the relatively high Fe/Mg ratio (Fig. 8) and the behavior of Nb, Zr, and Y, as displayed in the Meschede (1986) diagram (Fig. 10) for some rocks. Two groups of samples with basic and acid rocks with contrasting Ti contents were identified; we refer to them as low-Ti and high-Ti (Figs. 11 and 14).

Low-Ti basalts have lower amounts of Ba, Nb, Y, Zr, and REE (Fig. 6) and no negative Eu anomaly (Fig. 7), which may reflect the absence of large amounts of plagioclase in the fractionated phases. A lithospheric mantle source modified during previous subduction is suggested by high LREE/Nb ratios in the patterns normalized against N-type MORB values. A slight LREE enrichment relative to HREE occurs in roughly flat-normalized REE patterns, with La/Yb_N ratios of approximately 3–5, similar to those of mildly alkaline basalts from the Naivasha, Kenya, rift (Wilson, 1989).

High-Ti basic rocks are slightly enriched in most incompatible trace elements compared with low-Ti basalts (Fig. 6), and REE enrichment, higher LREE/HREE ratios ($La/Yb_N\approx10$–11), and small negative Eu anomalies are common features of this magmatism (Fig. 7). The compositional differences of high- and low-Ti basic magmas can be related to different melting fractions from an asthenospheric or lithospheric mantle (Baker et al., 1977) or within-plate, subduction-affected sources (Wilson, 1989). A few high-Ti basalt samples show slightly higher Nb contents ($\sim$18 ppm).

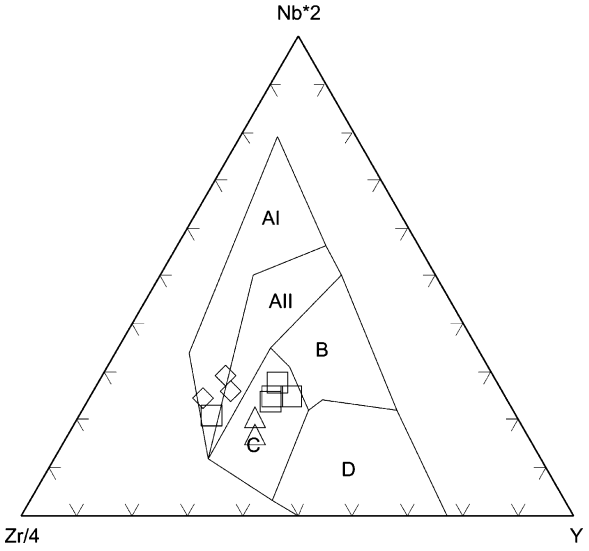

Fig. 10. Tectonic environment discrimination Zr/4–Y–Nb×2 diagram (Meschede, 1986) for intermediate and basic rock samples (data in ppm). AI–AII, within-plate alkaline basalts; AII–C, within-plate tholeiites; B, P-MORB; D, N-MORB; C–D, volcanic-arc basalts. Diamonds: shoshonitic intermediate lavas; triangles: low-Ti basic lavas and dykes; squares: high-Ti basic lavas and dykes.

Both high- and low-Ti types lie in the within-plate field on the TiO_2 versus Zr plot (Pearce, 1980) (Fig. 12). They show a transitional pattern compared with MORB-normalized patterns of within-plate tholeiitic and high-K basaltic magmas (Ewart, 1982; Pearce, 1982) (Fig. 13). This behavior is characteristic of basalts of transitional or moderately alkaline affinity, normally related to continental rifts or postcollisional settings (Leat et al., 1986). Basic magmatism with similar characteristics has been studied in the Campo Alegre basin (Waichel et al., 2000), Taquarembó Plateau (Wildner et al., 1999, 2002), and Santa Bárbara region (Almeida et al.. 2002) in the Neoproterozoic of southern Brazil, as well as the Avoca, Parys Mountain, and Snowdon provinces in the Paleozoic southern British Caledonides (Leat et al., 1986).

Acid rocks are dominantly high-silica types with SiO_2 values greater than 70 wt%, though a few samples show contents of 62–70 wt%. The acid rocks probably crystallized from peralkaline liquids and, due to the loss of alkali elements, show an agpaitic index close to 1 or lower. Zr contents, generally greater than 300 ppm, are consistent with this peralkaline affinity (Leat et al., 1986). The loss of alkaline elements can occur during crystallization or through postmagmatic alteration processes (Leat et al., 1986) and has been used by Sommer et al. (1999) to justify the peraluminous character of some acid volcanic rocks from the Taquarembó Plateau.

Three different groups of acid rocks were recognized in the Ramada Plateau according to the Zr/TiO_2, SiO_2, and Nb/Y parameters devised by Winchester and Floyd (1977) (Fig. 9). The first group plots in the rhyolite field; the others, coincident with high- and low-Ti types (Fig. 14), plot in the comendite/pantellerite field. In the low-Ti rhyolites, we also separate rocks with higher Nb and Y contents into a high-Nb rhyolite group. High-Ti acid rocks show a typical peralkaline character with an agpaitic index generally greater than 1 and low amounts of normative acmite. They do not plot in the comenditic/pantelleritic field, according to their higher Ti and lower Nb contents compared with comendites (Winchester and Floyd, 1977). Assuming a peralkaline character of both rhyolitic liquids, their comenditic affinity is confirmed on the $FeO_t \times Al_2O_3$ diagram (MacDonald, 1974a; Le Maitre, 2002) (Fig. 15). The behavior of the Ramada high- and low-Ti comendites in the Th versus Ta diagram (Fig. 16) is similar to typical comenditic associations such as Snowdon, Parys Mountain, Avoca (Leat et al., 1986), and Taquarembó Plateau (Sommer et al., 1999; Wildner et al., 1999). Nevertheless, high-Nb comendites show behavior transitional to more peralkaline compositions, with higher Ta contents, which is more common in pantelleritic associations (Hildreth, 1981).

Low-Ti Ramada comendites have higher Rb, Nb, and Y concentrations than those of high-Ti rocks, whereas high-Nb rhyolites show lower Fe and Ti and higher Nb, Rb, Y, and Ta contents than do high- and low-Ti acid rocks. Zr contents vary from 200 to 1200 ppm, though the highest values (>800 ppm) probably are related to the presence of cumulative zircon. Thus, we acknowledge that the acid liquids of the Ramada Plateau had Zr contents of approximately 350 ppm in the high-Nb group and 600 ppm for the high- and low-Ti groups. Zr variability in the acid rocks also is related to the agpaitic index (Watson and Harrison, 1983). Both types show contents typical of metaluminous alkaline to peralkaline acid associations, according to Leat et al. (1986).

In Fig. 17, we display trace-element patterns of rhyolites normalized against the granite ocean ridge granite values (Pearce et al., 1984), which show higher Ce and Sm values and lower Rb in the high-Ti rhyolites. Samples of high- and low-Ti and high-Nb rhyolites show similar patterns, with low Ba and Sr and high-field strength element (HFSE) values, consistent with the sodic-alkaline affinity of this sequence. The patterns of the high- and low-Ti rhyolites, with high Ce/Nb ratios, are similar to those of the postorogenic magmatic associations of the Snowdon rhyolites (Leat et al., 1986), whereas the high-Nb rhyolites patterns, with low Ce/Nb ratios, indicate an affinity with anorogenic magmatism, such as the Naivasha rhyolites of Kenya (MacDonald et al., 1987) (Fig. 18).

The chondrite-normalized REE patterns (Fig. 19) show an REE enrichment in the high-Ti rhyolites, particularly for LREE, with a La/Yb_N ratio of 10–12, whereas the low-Ti acid rocks present La/Yb_N ratio of 1–2. These patterns are coherent with those described in the high- and low-Ti basic rocks. The high-Nb rhyolites have strong LREE depletion, mainly in the most differentiated liquids, and a La/Yb_N ratio

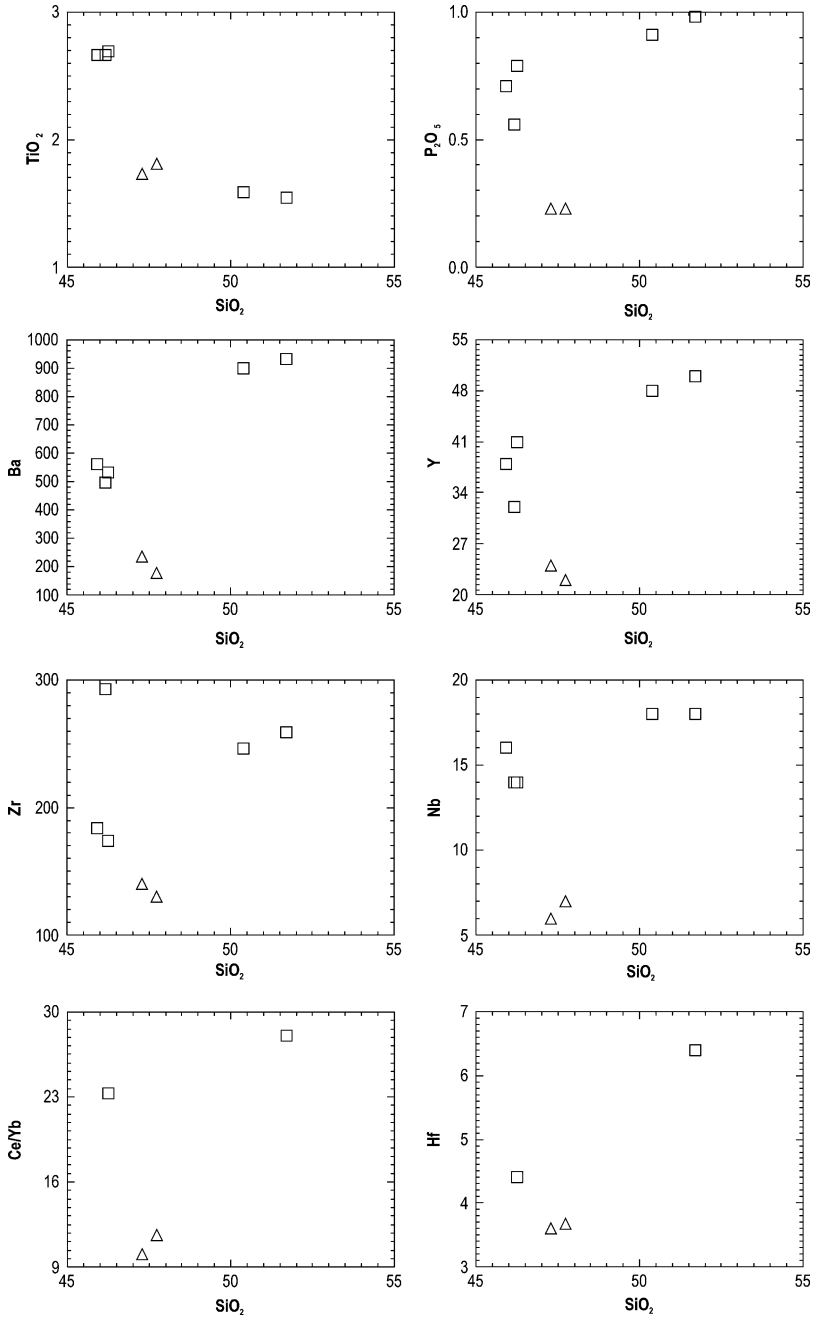

Fig. 11. Variation diagrams for major (in wt%) and trace elements (in ppm) for intermediate and basic rock samples. Triangles: low-Ti basic lavas and dykes; squares: high-Ti basic lavas and dykes.

close to 0.2–0.4. Strong negative Eu anomalies observed in both rhyolite groups, but greater in the high-Nb group, suggest feldspar fractionation. In the high-Nb rhyolites, the strong LREE depletion along the differentiation probably reflects the presence of LREE-rich minerals among the fractionated phases.

Almost all Ramada Plateau acid rocks plot in the within-plate granite field in the Y + Nb versus Rb and Y versus Nb diagrams (Pearce et al., 1984) (Fig. 20). The high- and low-Ti rhyolites plot mainly in the field of alkaline postcollisional magmatism, and the highest Nb, Y, and Rb values of the high-Nb rocks make them compositionally closer to anorogenic associations. Similar behavior is observed in the Zr versus Nb diagram (Fig. 21; Leat et al., 1986), in which the Zr/Nb ratios greater than 10 for the high- and low-Ti liquids point to magmatism related to sources modified by subduction in active continental margins or postcollisional settings (MacDonald, 1974a,b; Ewart, 1979; Leat et al., 1986). High-Nb rocks show Zr/Nb ratios less than 10, normally related to anorogenic settings

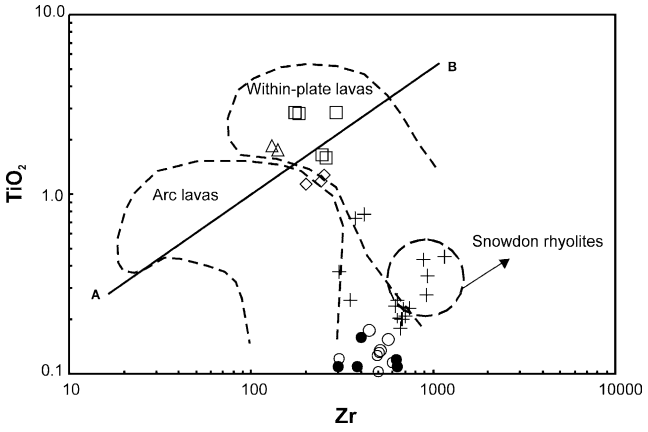

Fig. 12. Zr (ppm) versus TiO_2 (wt%) diagram showing fields of arc and within-plate lavas (modified from Pearce, 1980). Line A–B separates basic from intermediate-acid rocks; basic rocks are above the line. Snowdon rhyolite field obtained from Leat et al. (1986). Diamonds: shoshonitic intermediate lavas; triangles: low-Ti basic lavas and dykes; squares: high-Ti basic lavas and dykes; circles: low-Ti acid lavas, hypabyssal rocks, and ignimbrites; crosses: high-Ti acid lavas, hypabyssal rocks, and ignimbrites; and filled circles: high-Nb acid lavas, hypabyssal rocks, and ignimbrites.

such as the Naivasha rift volcanic association (MacDonald and Bailey, 1973).

The major-element composition of Ramada Plateau acid rocks, plotted in the chemical diagrams suggested by Patiño Douce (1999), is comparable to that of metaluminous to marginally peralkaline, A-type granites and rhyolites, despite the probable Na loss. However, their compositions are different from those produced by experimental melting of common crustal protoliths, which are slightly peraluminous, and those of rhyolites associated with plateau basalts (Patiño Douce, 1999).

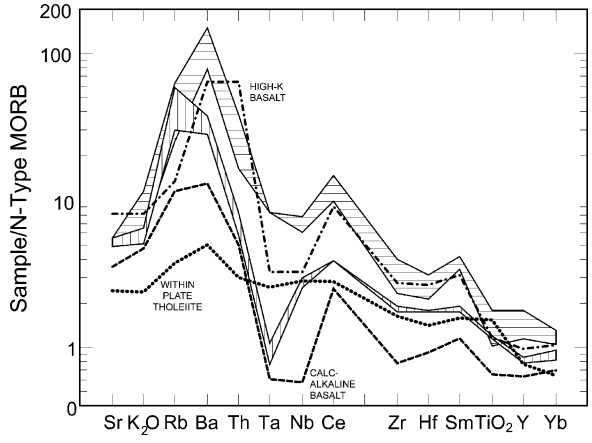

Fig. 13. N-MORB-normalized trace element spidergrams for basic rock samples compared with normalized patterns of within-plate tholeiitic and high-K basaltic magmas (modified from Leat et al., 1986). Field with vertical lines: low-Ti basic rocks; field with horizontal lines: high-Ti basic rocks.

6. Petrogenetic discussion

Ramada Plateau magmatism is characterized by a late Neoproterozoic, nondeformed association of basic and acid volcanic rocks and related subvolcanic intrusions, dykes, and sills. It is composed of a basal unit of shoshonitic intermediate lava flows and volcanogenic conglomerates, succeeded by a bimodal basic-acid association characterized by extensive rhyolitic pyroclastic flow deposits sometimes cut by basic dykes, and then followed by lava flows of acid and basic composition. Shallow rhyolitic–trachytic intrusions crosscut the country rocks around the Plateau.

The structures and textures observed in these deposits, the facies association in the Plateau, and the primary pyroclastic flow deposits with features of hot, gas-supported emplacement suggest volcanism in subaerial settings (McPhie et al., 1993). The association of these deposits with acid lava flows, which mostly occur along fissure zones where they exhibit a near-vertical flow foliation that gradates to autobrecciated facies and then to lavas with near-horizontal flow foliation and massive terms, suggests eruption through a fissural vent system. This suggestion is consistent with widespread dykes, sills, and other shallow intrusive bodies associated with a complex lineament system, which cut the country rocks. Lava flows have a geometry similar to *coulées*, which are formed when flow is asymmetric and concentrated on one side of the vent and produce an effusive deposit with geometry elongated in the plane (Cas and Wright, 1987). Eruption processes in the Ramada Plateau initially were dominated by explosive episodes that formed primary pyroclastic flows and were succeeded by lava flows and synvolcanic intrusions.

Basaltic trachyandesites of the basal unit are compositionally and texturally similar to intermediate volcanic rocks of the Neoproterozoic Lavras do Sul shoshonitic association (Lima and Nardi, 1998). The shoshonitic magmatism shows typical characteristics of a silica-saturated potassic alkaline series whose origin is related to subduction-modified sources in postcollisional settings (Lima and Nardi, 1998; Nardi and Lima, 2000). Available isotopic data for shoshonitic rocks in this region suggest Rb–Sr ages of 608 ± 54 Ma, an $^{87}Sr/^{86}Sr$ initial ratio of approximately 0.7048, and $\varepsilon\ Nd_{(T=600\ Ma)}$ values close to -0.2 (Gastal and Lafon, 1998), which indicate EM1-type lithospheric mantle sources. Pb–Pb ages of zircon from monzonitic rocks are 601 ± 5 Ma (Gastal and Lafon, 2001), and U–Pb isotopic data in zircon point to an age of 592 ± 5 Ma (Remus et al., 1997) for granitic rocks of this shoshonitic association.

The younger bimodal basic-acid volcanism belongs to a sodic, silica-saturated alkaline series, transitional to a continental tholeiitic one, as indicated by relatively high Fe/Mg ratios in the basic rocks and by the behavior of Nb, Zr, and Y in the Meschede (1986) diagram (Fig. 10). The alkaline association includes both high-Ti basalts/trachytes/rhyolites and low-Ti basalts/rhyolites. A high-Nb group also

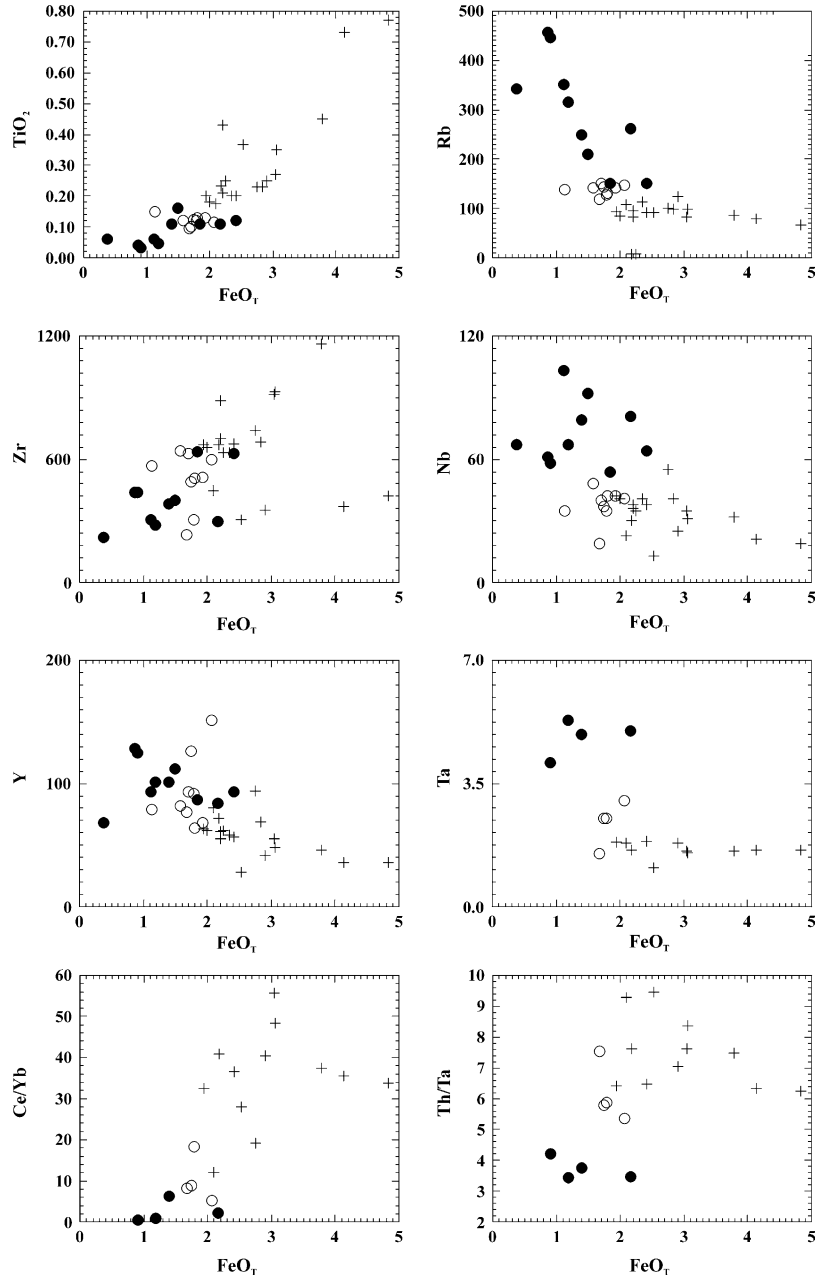

Fig. 14. Variation diagrams using FeO_t as differentiation index in relation to major (in wt%) and trace elements (in ppm) for acid rock samples. Circles: low-Ti acid lavas, hypabyssal rocks, and ignimbrites; crosses: high-Ti acid lavas, hypabyssal rocks, and ignimbrites; and filled circles: high-Nb acid lavas, hypabyssal rocks, and ignimbrites.

identified in the acid rocks probably is present among the basic rocks, though the few samples preclude a more precise characterization.

Low-Ti basalts have lower amounts of Ba, Nb, Y, Zr, and REE relative to the high-Ti basic rocks. Negative Nb anomalies relative to LREE in the patterns normalized against N-type MORB values indicate a lithospheric mantle source modified during previous subduction. A slight LREE enrichment relative to HREE is observed on roughly flat-normalized REE patterns, with La/Yb_N ratios similar to those of mildly alkaline basalts (Wilson, 1989).

Both high- and low-Ti types lie in the within-plate field in the TiO_2 versus Zr plot (Pearce, 1980), characteristic of transitional or moderately alkaline basalts and generally related to continental rifts or postcollisional settings (Leat et al., 1986). The compositional differences of high- and low-Ti basic magmas can be related to different melt fractions derived from an asthenospheric or lithospheric mantle (Baker et al., 1977; Wilson, 1989).

Acid rocks partially preserve the characteristics of the so-called trivially peralkaline (MacDonald et al., 1987) liquids; however, they are probably comenditic, as indicated by

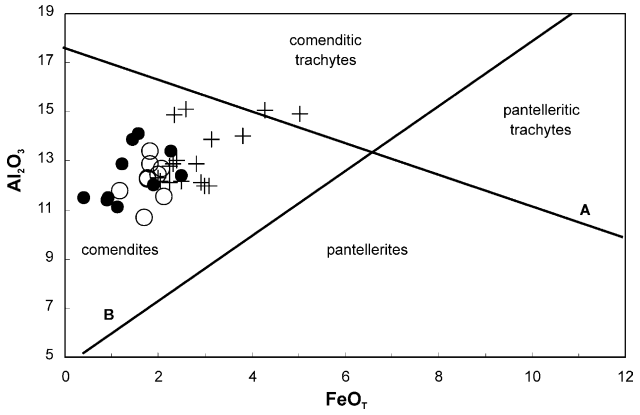

Fig. 15. Ramada Plateau acid rock samples plotted in the Al_2O_3 versus FeO_t diagram (MacDonald, 1974a). The boundary lines separate the field of trachytes from rhyolites (line A) and comenditic from pantelleritic (line B) rocks. Data plotted in wt%. Circles: low-Ti acid lavas, hypabyssal rocks, and ignimbrites; crosses: high-Ti acid lavas, hypabyssal rocks, and ignimbrites; and filled circles: high-Nb acid lavas, hypabyssal rocks, and ignimbrites.

the high (generally >300 ppm) Zr contents (Leat et al., 1986). The agpaitic index does not reflect their peralkalinity because of the loss of alkali elements during crystallization, as has been observed in other acid-volcanic associations. Three groups of acid rocks—high-Ti, low-Ti, and high-Nb—can be discriminated in the Ramada Plateau according to diagrams that compare Zr/TiO_2 and Nb/Y ratios. The comenditic affinity of both rhyolitic liquids is confirmed by the $FeO_t \times Al_2O_3$ diagram (MacDonald, 1974a; Le Maitre, 2002).

Low-Ti Ramada comendites are characterized by higher Rb, Nb, and Y values and lower Zr, Ce, and Sm contents

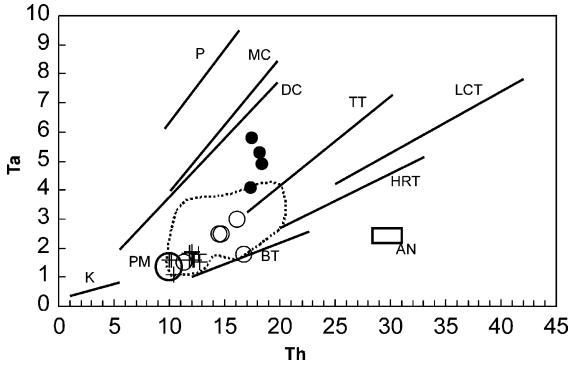

Fig. 16. Th versus Ta diagram (modified from Hildreth, 1981; Leat et al., 1986) for acid rock samples (data in ppm). Lines represent generalized trends of large silicic eruptive units. P: Pantelleria, Italy; MC: Menengai, Kenya; DC: Devine Canyon Tuff, Oregon, USA; TT: Tala Tuff, Mexico; LCT: Lava Creek Tuff and HRT: Huckleberry Ridge Tuff, both in Yellowstone, USA; BT: Bishop Tuff, California, USA; K: Katmai, Alaska, USA; AN: comendite, Peru; PM: Parys Mountain, southern British Caledonides. Pointed line: Taquarembó Plateau acid volcanic rocks field. Circles: low-Ti acid lavas, hypabyssal rocks, and ignimbrites; crosses: high-Ti acid lavas, hypabyssal rocks, and ignimbrites; and filled circles: high-Nb acid lavas, hypabyssal rocks, and ignimbrites.

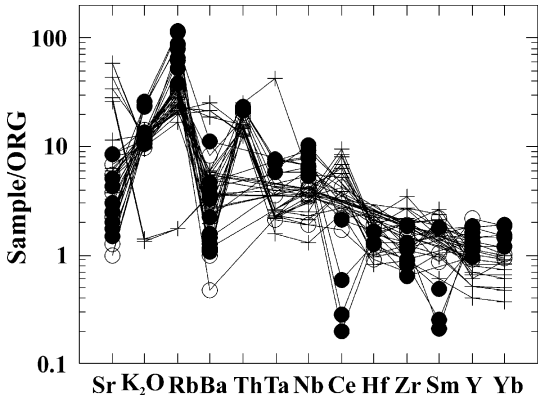

Fig. 17. Ocean ridge granite-normalized trace-element spidergrams for acid rock samples. Circles: low-Ti acid lavas, hypabyssal rokcs, and ignimbrites; crosses: high-Ti acid lavas, hypabyssal rocks, and ignimbrites; and filled circles: high-Nb acid lavas, hypabyssal rocks, and ignimbrites.

than are high-Ti rocks. High-Nb rhyolites present lower Fe and Ti and higher Nb, Y, Rb, and Ta contents than either high- or low-Ti rocks. Both types show Zr contents typical of alkaline-metaluminous to peralkaline acid associations (Leat et al., 1986). An REE enrichment is observed in the high-Ti rhyolites, particularly for LREE, whereas the low-Ti acid rocks have flatter patterns that are coherent with those described for the high- and low-Ti basic rocks. Therefore, the REE patterns suggest the comagmatic character of low-Ti basic-acid liquids and high-Ti basic-intermediate acid liquids. High-Nb rocks have strong LREE depletion in most differentiated liquids.

Alkaline or mildly alkaline basalts and comendites in bimodal associations can be related to different tectonic settings (MacDonald, 1974a,b; Civetta et al., 1998). The three most important settings are (1) anorogenic continental areas with doming and rifting processes (e.g. Kenya rift,

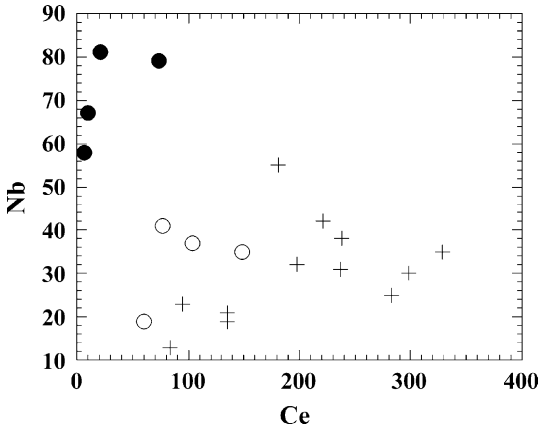

Fig. 18. Ce versus Nb diagram for acid rock samples. Circles: low-Ti acid lavas, hypabyssal rocks, and ignimbrites; crosses: high-Ti acid lavas, hypabyssal rocks, and ignimbrites; and filled circles: high-Nb acid lavas, hypabyssal rocks, and ignimbrites.

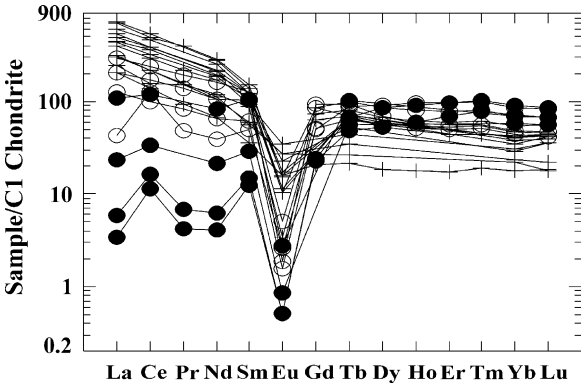

Fig. 19. Chondrite-normalized REE patterns for acid rock samples. Circles: low-Ti acid lavas, hypabyssal rocks, and ignimbrites; crosses: high-Ti acid lavas, hypabyssal rocks, and ignimbrites; and filled circles: high-Nb acid lavas, hypabyssal rocks, and ignimbrites.

MacDonald and Bailey, 1973; Black et al., 1997; Pantelleria Island, Italy, Civetta et al., 1998); (2) oceanic islands tectonically related to oceanic chains (e.g. Socorro Island, Pacific coast of Mexico, Bohrson and Reid, 1997;

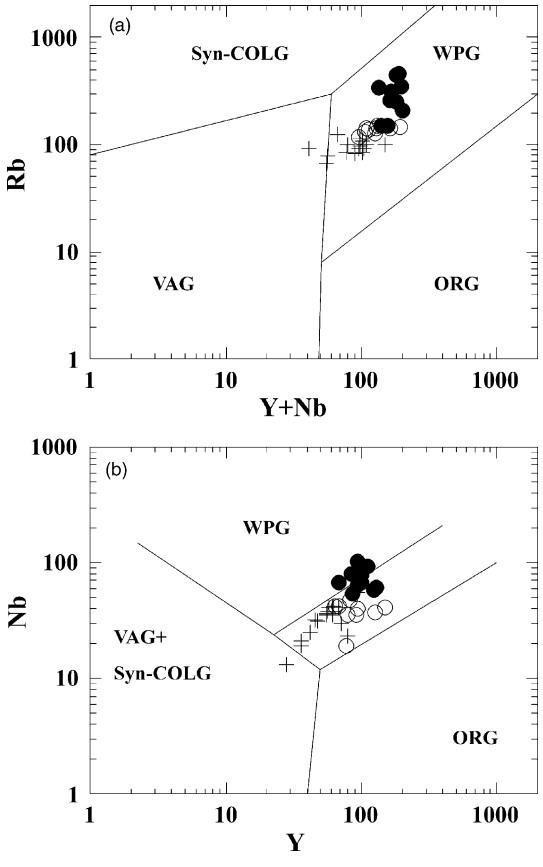

Fig. 20. Tectonic environment discrimination diagrams (Pearce et al., 1984) for acid rock samples (data in ppm). (a) Y + Nb versus Rb diagram, and (b) Y versus Nb diagram. Syn-Colg, syncollision granites; VAG, volcanic arc granites; WPG, within-plate granites; ORG, ocean ridge granites. Circles: low-Ti acid lavas, hypabyssal rocks, and ignimbrites; crosses: high-Ti acid lavas, hypabyssal rocks, and ignimbrites; and filled circles: high-Nb acid lavas, hypabyssal rocks, and ignimbrites.

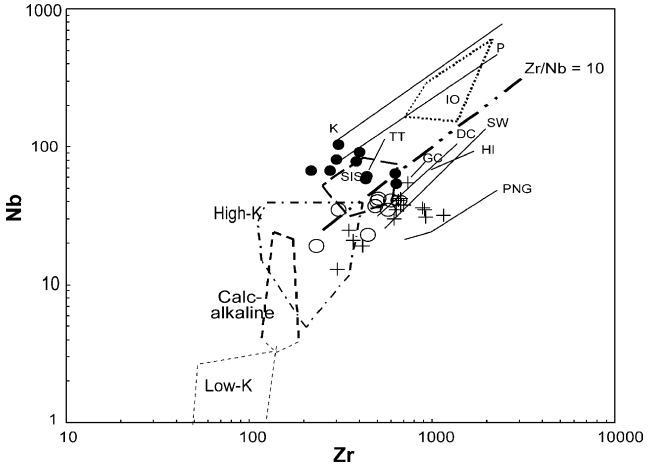

Fig. 21. Tectonic environment discrimination Zr×Nb diagram (modified from Leat et al., 1986) for studied rock samples (data in ppm). SIS, perthite granite from Lavras do Sul granitic complex and peralkaline granite of Dom Pedrito, Rio Grande do Sul State, Brazil, associated with Saibro intrusive suite (from Gastal et al., 1992). The following fields were obtained from Leat et al. (1986): SW: Snowdon rhyolites; PNG: Papau New Guinea; HI: Mayor Island, New Zealand; DC: Devine Canyon Tuff; GC: Grouse Canyon Tuff, Silent Canyon Centre, Nevada; TT: Tala Tuff, La Primavera Centre, Mexico; P: Pantelleria; K: Kilombe, Kenya; IO: Ocean Islands. Circles: low-Ti acid lavas, hypabyssal rocks, and ignimbrites; crosses: high-Ti acid lavas, hypabyssal rocks, and ignimbrites; and filled circles: high-Nb acid lavas, hypabyssal rocks, and ignimbrites.

Thverartindur volcanic complex, Iceland, Soesoo, 1997); and (3) bimodal associations related to the final stages of orogenic cycles with extensional tectonics (Parys Mountain and Snowdon, southern British Caledonides, Leat et al., 1986; Taquarembó Plateau, Wildner et al., 1999; Campo Alegre basin, Waichel et al., 2000). In this last setting, the postcollisional peralkaline volcanic rocks are approximately coeval with calc-alkaline or shoshonitic associations, as noted by Smith et al. (1977) and Smith and Johnson (1981).

In a broad sense, the characteristics of the Ramada Plateau shoshonitic to mildly alkaline sodic magmatism suggest it evolved from different parental magmas, whose diversity can be related to mantle compositional heterogeneities or different fraction melts from the same source previously affected by subduction-related metasomatism. The anorogenic character of the high-Nb parental magmas is ascribed to the decrease of subduction-related metasomatism effects or an increasing asthenospheric contribution. Atherton and Ghani (2002) propose a model of magma generation in collisional settings, which involves slab break off and asthenospheric upwelling, that could be applied to the magmatism evolution from subduction-related to anorogenic in the Ramada Plateau.

Mantle sources for the parental magmas of many shoshonitic and alkaline magmatic associations related to Ramada magmatism are assumed by most authors (Nardi, 1984; Nardi and Bonin, 1991; Gastal and Lafon, 1998; Lima and Nardi, 1998; Wildner et al., 1999). Isotopic data

obtained from rocks of the Taquarembó Plateau Neoproterozoic plutonovolcanic alkaline association (Wildner et al., 1999) suggest an EM1-type mantle source, as defined by Hart (1988). Nd and Sr data determined from lavas (Chemale et al., 1999) yield $\varepsilon Nd_{(T=570\ Ma)}$ values between −15 and −17 and $(Sr_{87}/Sr_{86})_i$ close to 0.7045, similar to data obtained by Gastal and Lafon (1998) for intrusive rocks of alkaline associations related to the Taquarembó Plateau magmatism.

The origin of acid alkaline magmas generally has been ascribed to partial crustal melting (Whalen et al., 1987; MacDonald et al., 1987) or fractional crystallization of basic or intermediate magmas (Bonin, 1986; Shannon et al., 1997; Sommer et al., 1999). The former hypothesis lacks the support of experimental petrology; the production of peralkaline liquids through partial melting of metamorphic rocks has not been proved. In addition, it explains neither the trace element similarities of basaltic and rhyolitic rocks nor their moderate to high HFSE contents. The trachytic and rhyolitic rocks of the Ramada Plateau can be generated by fractional crystallization of mildly alkaline basaltic magmas. Sommer et al. (1999) model the evolution of a similar trachyte–rhyolite association by fractional crystallization. Alternatively, a reaction model among basaltic and metamorphic rocks is possible. Patiño Douce (1999) suggests generation of metaluminous to slightly peralkaline magmas by the interaction of aluminous basaltic magmas and calc-alkaline metamorphic rocks, which seems an adequate genetic model for the studied rhyolitic liquids. The model could be improved by including a mildly alkaline basalt instead of an aluminous one and extensive plagioclase fractionation to explain the comenditic character and enriched trace-element patterns.

7. Final considerations

Neoproterozoic volcanism in the Ramada Plateau presents facies associations that suggest a subaerial, fissural volcanic regime represented by shoshonitic intermediate lavas, dominantly acid pyroclastic flows, and acid-basic effusive deposits of mildly alkaline affinity. This bimodal association presents low- and high-Ti compositions that seem to evolve to anorogenic magmatic associations with high-Nb contents. This evolution marks the final stages of postcollisional magmatism in southernmost Brazil and probably reflects the change of magmatic sources from subduction-related to continental within-plate or anorogenic settings.

Acknowledgements

This work was supported financially by PRONEX-UFRGS, FAPERGS (00/0173.9, 01/1103.5, and BIC 00512023) and CNPq (4700181/01-5). The authors are grateful to CPGq-UFRGS and the Brazilian Geological Survey-CPRM (SUREG PA) for logistical support. The manuscript was much improved by revisions by Drs Eric H. Christiansen, Valdecir Janasi, and Roberto Dall'Agnol.

References

Almeida, D.P.M., Zerfass, H., Basei, M.A., Petry, K., Gomes, C.H., 2002. The Acampamento Velho Formation, a Lower Cambrian bimodal volcanic package: geochemical and stratigraphic studies from the Cerro do Bugio, Perau and Serra de Santa Bárbara, Caçapava do Sul, Rio Grande do Sul, RS-Brazil. Gondwana Research 5 (3), 721–733.

Atherton, M.P., Ghani, A.A., 2002. Slab breakoff: a model for Caledonian, late granite syn-collisional magmatism in the orthotectonic (metamorphic) zone of Scotland and Donegal, Ireland. Lithos 62 (3/4), 65–85.

Babinski, M., Chemale Jr.., F., Van Schmus, W.R., Hartmann, L.A., Silva, L.C., 1997. U–Pb and Sm–Nd geochronology of the Neoproterozoic granitic-gneissic Dom Feliciano belt, southern Brazil. Journal of South American Earth Sciences 10, 263–274.

Baker, B.H., Goles, G.G., Leeman, W.P., Lindstrom, M.M., 1977. Geochemistry and petrogenesis of a basalt–benmoreite–trachyte suite from the southern part of the Gregory Rift, Kenya. Contributions to Mineralogy and Petrology 64, 303–332.

Bitencourt, M.F., Nardi, L.V.S., 2000. Tectonic setting and sources of magmatism related to the southern Brazilian shear belt. Revista Brasileira de Geociências 30, 186–189.

Black, S., MacDonald, R., Kelly, M.R., 1997. Crustal origin for peralkaline rhyolites from Kenya: evidence from U-series disequilibria and Th-isotopes. Journal of Petrology 38, 277–297.

Bohrson, W.A., Reid, M.R., 1997. Genesis of silicic peralkaline volcanic rocks in an ocean island setting by crustal melting and open-system processes: Socorro Island, Mexico. Journal of Petrology 38, 1137–1166.

Bonin, B., 1986. Ring Complex Granites and Anorogenic Magmatism. North Oxford Academic Publishers, London. 189 pp.

Brito Neves, B.B., Cordani, U.G., 1991. Tectonic evolution of South America during Late Proterozoic. Precambrian Research 53, 23–40.

Cas, R.A.F., Wright, J.V., 1987. Volcanic Succession, Modern and Ancient: A Geological Approach to Processes, Products and Successions. Allen & Unwin, London. 528 pp.

Chemale Jr.., F., 2000. Evolução geológica do Escudo Sul-rio-grandense, in: Holz, M., De Ros, L.F. (Eds.), Geologia do Rio Grande do Sul. Volume Especial, CIGO/UFRGS, Porto Alegre, pp. 13–52.

Chemale Jr., F., Wildner, W., Lima, E.F., Van Schmus, W.R., 1999. Isotopic studies of Brasiliano retro-arc magmatism in southern Brazil. Boletim de Resumos, Simpósio sobre Vulcanismo e Ambientes Associados 1, Gramado, SBG/Núcleo Sul, 57.

Civetta, L., D'Antonio, M., Orsi, G., Tilton, G.R., 1998. The geochemistry of volcanic rocks from Pantelleria Island, Sicily Channel: petrogenesis and characteristics of the mantle source region. Journal of Petrology 39, 1453–1491.

Compston, W., Willians, I.S., Meyer, C., 1984. Geochronology of zircons from the lunar breccia 73217 using a sensitive high mass resolution ion microprobe. Journal of Geophysical Research 89, 525–534.

Compston, W., Willians, I.S., Kirschvink, J.L., Zichao, Z.H., Guogan, M., 1992. Zircon ages for the Early Cambrian time-scale. Journal of the Geological Society, London 149, 171–184.

Ewart, A., 1979. A review of the mineralogy and chemistry of Tertiary-Recent dacitic, latitic, rhyolitic and related salic volcanic rocks, in: Baker, F. (Ed.), Trondhjemites, Dacites and Related Rocks. Elsevier, The Netherlands, pp. 113–121.

Ewart, A., 1982. The mineralogy and petrology of Tertiary-Recent orogenic volcanic rocks with special reference to the andesitic–basaltic

compositional range, in: Thorpe, R.S. (Ed.), Andesites. Wiley, New York, pp. 25–87.

Fernandes, L.A.D., Tommasi, A., Porcher, C.C., 1992. Deformation patterns in the southern Brazilian branch of the Dom Feliciano belt: a reappraisal. Journal of South American Earth Sciences 5 (1), 77–96.

Gastal, M.C.P., Lafon, J.M., 1998. Gênese e evolução dos granitóides metaluminosos de afinidade alcalina da porção oeste do escudo sul-rio-grandense: Geoquímica e isótopos de Rb–Sr e Pb–Pb. Revista Brasileira de Geociências 28, 11–28.

Gastal, M.C.P., Lafon, J.M., 2001. Novas idades $^{207}Pb/^{206}Pb$ e geoquímica isotópica Nd–Sr para granitóides shoshoníticos e alcalinos das regiões de Lavras do Sul e Taquarembó, RS. Anais VIII Congresso Brasileiro de Geoquímica, Curitiba, SBGq 2001;, 21–26.

Gastal, M.C.P., Schmitt, R.S., Nardi, L.V.S., 1992. Granitóides da parte centro-sudoeste do Escudo Sul-rio-grandense: Novos dados e discussão sobre a gênese e tipologia do magmatismo alcalino. Pesquisas 19 (2), 174–182.

Hart, S.R., 1988. Heterogeneous mantle domains: signatures, genesis and mixing chronologies. Earth Planetary and Science Letters 90, 273–296.

Hartmann, L.A., Nardi, L.V.S., Formoso, M.L.L., Remus, M.V.D., Lima, E.F., Mexias, A.S., 1999. Magmatism and metallogeny in the crustal evolution of Rio Grande do Sul Shield, Brazil. Pesquisas 26 (2), 45–63.

Hildreth, W., 1981. Gradients in silicic magma chambers: implications for lithospheric magmatism. Journal of Geophysical Research 86, 10153–10192.

Irvine, T.N., Baragar, W.R.A., 1971. A guide to the chemical classification of the common volcanic rocks. Canadian Journal of Earth Sciences 8, 523–548.

Kelemen, P.B., Shimizu, N., Dunn, T., 1993. Relative depletion of niobium in some arc magmas and the continental crust: partitioning of K, Nb, La and Ce during melt/rock reaction in the upper mantle. Earth and Planetary Science Letters 120, 111–134.

Leake, B.E., Woolley, A.R., Arps, C.E.S., Birch, W.D., Gilbert, M.C., Grice, J.D., Hawthorne, F.C., Kato, A., Kisch, H.J., Krivovichev, V.G., Linthout, K., Laird, J., Mandarino, J.A., Maresch, W.V., Nickel, E.H., Rock, N.M.S., Schumacher, J.C., Smith, D.C., Stephenson, N.C.N., Ungaretti, L., Whittaker, E.J.W., Youzhi, G., 1997. Nomenclature of amphiboles: report of the subcommittee on amphiboles of the International Mineralogical Association, commission on new minerals and mineral names. The Canadian Mineralogist 35, 219–246.

Leat, P.T., Jackson, S.E., Thorpe, R.S., Stillman, C.J., 1986. Geochemistry of bimodal basalt—subalkaline/peralkaline rhyolite provinces within the southern British Caledonides. Journal of the Geological Society, London 143, 259–273.

Le Bas, M.J., Le Maitre, R.W., Streckeisen, A., Zanettin, B., 1986. A classification of volcanic rocks based on the total alkali–silica diagram. Journal of Petrology 27, 745–750.

Le Maitre, R.W., 2002. Igneous rocks: a classification and glossary of terms. In: Recommendations of the International Union of Geological Sciences Subcommission on the Systematic of Igneous Rocks, second ed. Cambridge University Press, Cambridge, 252 pp.

Liégeois, J.P., 1998. Preface: some words on post-collisional magmatism. Lithos 45, 15–17.

Lima, E.F., Nardi, L.V.S., 1998. The Lavras do Sul shoshonitic association: implications for the origin and evolution of Neoproterozoic shoshonitic magmatism in the southernmost Brazil. Journal of South American Earth Sciences 11 (1), 67–77.

Lofgren, G., 1971. Spherulitic textures in glassy and crystalline rocks. Journal of Geophysical Research 76, 5635–5648.

Lofgren, G., 1974. An experimental study of plagioclase crystal morphology: isothermal crystallisation. American Journal of Science 274, 243–273.

MacDonald, R., 1974a. Nomenclature and petrochemistry of the peralkaline oversaturated extrusive rocks. Bulletin Volcanologique 38 (3), 498–516.

MacDonald, R., 1974b. Tectonic settings and magma associations. Bulletin Volcanologique 38 (3), 575–593.

MacDonald, R., Bailey, D.K., 1973. The chemistry of the peralkaline oversaturated obsidians. US Geological Survey Professional Paper 440-N-1, 1–37.

MacDonald, R., Davies, G.R., Bliss, C.M., Leat, P.T., Bailey, D.K., Smith, R.L., 1987. Geochemistry of high-silica peralkaline rhyolites, Naivasha, Kenya rift valley. Journal of Petrology 28 (6), 979–1008.

Matos, D.F., Lima, E.F., Sommer, C.A., Nardi, L.V.S., Liz, J.D., Figueiredo, A.M.G., Waichel, B.L., Pierosan, R., 2002. Riolitos neoproterozóicos pós-colisionais na área do Santuário, sul do Brasil: Litoquímica, química mineral e origem das heterogeneidades texturais. Revista Brasileira de Geociências 32 (2), 255–266.

McPhie, J., Doyle, M., Allen, R., 1993. Volcanic Textures. A Guide to the Interpretation of Textures in Volcanic Rocks. Centre for Ore Deposit and Exploration Studies, University of Tasmania, 198 pp.

Meschede, M., 1986. A method of discriminating between different types of mid-ocean ridge basalts and continental tholeiites with the Nb–Zr–Y diagram. Chemical Geology 56 (3/4), 207–218.

Mitchell, R.H., 1990. A review of the compositional variation of amphiboles in the alkaline plutonic complexes. Lithos 26, 135–156.

Morimoto, C.N., 1988. Nomenclature of pyroxenes. Mineralogical Magazine 52, 535–550.

Morrison, G.W., 1980. Characteristics and tectonic setting of the shoshonite rock association. Lithos 13, 97–108.

Nardi, L.V.S., 1984. Geochemistry and Petrology of the Lavras Granite Complex, RS, Brasil. Tese de Doutorado, Londres, Universidade de Londres, 268 pp.

Nardi, L.V.S., Bitencourt, M.F., 1989. Geologia, petrologia e geoquímica do Complexo Granítico de Caçapava do Sul, RS. Revista Brasileira de Geociências 19 (2), 153–169.

Nardi, L.V.S., Bonin, B., 1991. Post-orogenic and non-orogenic alkaline granite associations: the Saibro intrusive suite, southern Brazil—a case study. Chemical Geology 92, 197–212.

Nardi, L.V.S., Lima, E.F., 2000. O magmatismo shoshonítico e alcalino da Bacia do Camaquã, RS, in: Holz, M., De Ros, L.F. (Eds.), Geologia do Rio Grande do Sul. Volume Especial, CIGO/UFRGS, Porto Alegre, pp. 119–131.

Nicholls, J., Carmichael, I.S.E., 1969. Peralkaline acid liquids: a petrological study. Contributions to Mineralogy and Petrology 20, 268–294.

Paim, P.S.G., Chemale Jr.., F., Lopes, R.C., 2000. A Bacia do Camaquã, in: Holz, M., De Ros, L.F. (Eds.), Geologia do Rio Grande do Sul. Volume Especial, CIGO/UFRGS, Porto Alegre, pp. 231–374.

Patiño Douce, A., 1999. What do experiments tell us about the relative contributions of crust and mantle to the origin of granitic magmas?, in: Castro, A., Fernandez, C., Vigneresse, J.L. (Eds.), Understanding Granites: Integrating New and Classical Techniques Geological Society of London, Special Publications, 168, pp. 55–75.

Pearce, J.A., 1980. Geochemical evidence for the genesis and eruptive setting of lavas from the Tethyan ophiolites. Proceedings of the International Ophiolite Symposium, Nicosia, Cyprus 1980;, 261–272.

Pearce, J.A., 1982. Trace elements characteristics of lavas from destructive plate boundaries, in: Thorpe, R.S. (Ed.), Andesites: Orogenic Andesites and Related Rocks. Wiley, New York, pp. 525–546.

Pearce, J.A., Harris, N.B.W., Tindle, A.G., 1984. Trace element discrimination diagrams for the tectonic interpretation of granitic rocks. Journal of Petrology 25 (4), 956–983.

Phillip, R.P., Nardi, L.V.S., Bitencourt, M.F., 2000. O Batólito Pelotas no Rio Grande do Sul, in: Holz, M., De Ros, L.F. (Eds.), Geologia do Rio Grande do Sul. Volume Especial, CIGO/UFRGS, Porto Alegre, pp. 133–160.

Remus, M.V.D., McNaughton, N.J., Hartmann, L.A., Fletcher, I.R., 1997. Zircon SHRIMP dating and Nd isotope data of granitoids of the São Gabriel Block, southern Brazil: evidence of an Archaean/Paleoproterozoic basement. Extended Abstracts, International Symposium on Granites and Associated Mineralization 2, Salvador 1, pp. 217–272.

Rocha, F.F.N., Lima, E.F., Prado, M., Bastos Neto, A., Matos, D.F., 1999. Mineralizações de fluorita e galena em derrames riolíticos da região de Vila Nova (Aloformação Acampamento Velho), RS: Resultados preliminares. Boletim de Resumos, Simpósio sobre Vulcanismo e Ambientes Associados 1, Gramado, SBG/Núcleo Sul, 84.

Shannon, W.M., Barnes, C.G., Bickford, M.E., 1997. Grenville magmatism in West Texas: petrology and geochemistry of the Red Bluff Granitic Suite. Journal of Petrology 38 (10), 1297–1305.

Sheridan, M.F., 1970. Fumarolic mounds and ridges of the Bishop Tuff, California. Geological Society of America Bulletin 81, 851–868.

Smith, I.E.M., Johnson, R.W., 1981. Contrasting rhyolite suites in the Late Cenozoic of Papua New Guinea. Journal of Geophysical Research 86, 10257–10272.

Smith, I.E.M., Chappell, B.W., Ward, G.K., Freeman, R.S., 1977. Peralkaline rhyolites associated with andesitic arcs of the southwest Pacific. Earth and Planetary Science Letters 37, 230–236.

Soesoo, A., 1997. Oceanic magmatism and diverse plutonic products within the Thverarindur central volcanic complex at the former Icelandic plate margin. Journal of the Geological Society, London 154, 483–489.

Soliani Jr.., E., Koester, E., Fernandes, L.A.D., 2000. A geologia isotópica do Escudo Sul-rio-grandense. Parte II. os dados isotópicos e interpretações petrogenéticas, in: Holz, M., De Ros, L.F. (Eds.), Geologia do Rio Grande do Sul. Volume Especial, CIGO/UFRGS, Porto Alegre, pp. 175–230.

Sommer, C.A., Lima, E.F., Nardi, L.V.S., 1999. Evolução do vulcanismo alcalino na porção sul do Platô do Taquarembó, Dom Pedrito, RS. Revista Brasileira de Geociências 29 (2), 245–254.

Sommer, C.A., Lima, E.F., Nardi, L.V.S., Liz, J.D., Matos, D., 2001. Ignimbritos ricos em cristais do Platô da Ramada, RS, Brasil. Actas de resumos expandidos (meio digital), Congresso Latinoamericano de Geologia, XI, Montevideu, Uruguai.

Strong, D.F., Taylor, R.P., 1984. Magmatic-subsolidus and oxidation trends in compositions of amphiboles from silica-saturated peralkaline igneous rocks. Tschermarks Mineralogische und Petrologische Mitteilungen 32, 211–222.

Sutherland, D.S., 1975. Petrography and mineralogy of the peralkaline silicic rocks. Bulletin of Volcanology 38 (3), 517–547 (special issue).

Waichel, B., Lima, E.F., Nardi, L.V.S., Sommer, C.A., 2000. The alkaline post-collisional volcanism of Campo Alegre Basin in southern Brazil: petrogenetic aspects. Revista Brasileira de Geociências 30 (3), 393–396.

Watson, E.B., Harrison, T.M., 1983. Zircon saturation revisited: temperature and composition effects in a variety of crustal magma types. Earth and Planetary Science Letters 64, 295–304.

Whalen, J.B., Currie, K.L., Chappell, B.W., 1987. A-type granites: geochemical characteristics, discrimination and petrogenesis. Contributions to Mineralogy and Petrology 95, 407–419.

Wildner, W., Nardi, L.V.S., Lima, E.F., 1999. Post-collisional alkaline magmatism on the Taquarembó Plateau: a well-preserved Neoproterozoic-Cambrian plutono-volcanic association in southern Brazil. International Geology Review 41, 1082–1098.

Wildner, W., Lima, E.F., Nardi, L.V.S., Sommer, C.A., 2002. Volcanic cycles and setting in the Neoproterozoic III to Ordovician Camaquã Basin succession in southern Brazil: characteristics of post-collisional magmatism. Journal of Volcanology and Geothermal Research 118, 261–283.

Wilson, M., 1989. Igneous Petrogenesis. Unwin Hyman, London. 466 pp.

Winchester, J.A., Floyd, P.A., 1977. Geochemical discrimination of different magma series and their differentiation products using immobile elements. Chemical Geology 20, 325–343.